Design and Fabrication of Non-Noble-Metal Electrocatalysts for Oxygen Reduction Reactions

Ji Liang

School of Chemical Engineering

A thesis submitted for the degree of Doctor of Philosophy

The University of Adelaide

Jul 2014

Table of Contents

Abstract

Fuel cell is a device that can directly convert the chemical energy in fuels into electricity and it has the advantages including high efficiency, high energy density and zero waste emission. However, a current fuel cell requires noble-metal catalysts (in most cased platinum, Pt) to accelerate the electrode reactions. As a result of the high cost of Pt, the commercialization of fuel cell has been severely hindered. Thus, it is exceptionally important to search for an alternative low-cost catalyst, especially on the cathode when the sluggish oxygen reduction reaction (ORR) occurs and much larger amount of Pt is employed, to bring down the over-all price of a fuel cell. With this aim, this Ph.D thesis has demonstrated the design and synthesis of a serial of high –performance Pt-free catalysts based on carbon materials. These researches include:

(1) We firstly designed and constructed a series of porous g-C_3N_4/C composite with different pore size ranging from large mesopores (*ca.* 12 nm) to large macropores (*ca.* 400 nm) and studied the structural impact of these hybrid materials on their ORR performance. In this study, we have for the first time revealed that macropores would be more favorable for ORR in such materials rather than the conventionally believed mesopores.

(2) Then, we integrated short-range ordered mesopores into the walls of macropores to form a hierarchical pore structure. By incorporating graphene into this system, its electric conductivity can be enhanced. This is the first study to natively grow graphene on porous carbon. It is found that this material shows an excellent ORR performance with synergistically enhanced activities. Tafel analysis confirms that the good performance was brought from its unique structural advantages.

(3) To further enhance the catalytic activity of the above materials with ideal hierarchical structures for ORR, we have introduced high active Fe-N species into the system during the fabrication. By delicate tuning of the Fe content, we are able to control the carbon nano-materials on the hierarchical porous carbon to form graphene or carbon nanotube. As a result, the catalyst has obtained a similarity high performance as Pt as a result of the successful combination of the desired merits for ORR on it.

(4) Besides the optimization of materials structure, we have also doped graphene with both N and S, and studied the influence of dual dopants on its ORR activity. We found that a significant performance enhancement was achieved by dual-doping. From density function theory calculation, we found the synergistic effect was from the spin and charge densities redistribution brought by dual-doping of S and N, leading to a larger number of ORR active sites.

The studies in this thesis have provided a thorough understand of the kinetic and mechanism of the ORR process on the Pt-free catalysts. The research has not only provided materials with optimized structure and high performance for ORR, but also showed an avenue on the materials' design and construction for further study.

Thesis Declaration Statement by Author

I certify that this work contains no material which has been accepted for the award of any other degree or diploma in my name, in any university or other tertiary institution and, to the best of my knowledge and belief, contains no material previously published or written by another person, except where due reference has been made in the text. In addition, I certify that no part of this work will, in the future, be used in a submission in my name, for any other degree or diploma in any university or other tertiary institution without the prior approval of the University of Adelaide and where applicable, any partner institution responsible for the joint-award of this degree.

I give consent to this copy of my thesis when deposited in the University Library, being made available for loan and photocopying, subject to the provisions of the Copyright Act 1968.

The author acknowledges that copyright of published works contained within this thesis resides with the copyright holder(s) of those works.

I also give permission for the digital version of my thesis to be made available on the web, via the University's digital research repository, the Library Search and also through web search engines, unless permission has been granted by the University to restrict access for a period of time.

Name of Candidate: Ji Liang

Signature:

Date: 2014/7/14

Acknowledgement

First and foremost, I would like to express my most sincere gratitude to my principle supervisor Prof. Shizhang Qiao and co-supervisor Prof. Mark James Biggs, for their invaluable and continuous guidance of my Ph.D research and study, without which it would be impossible to have the achievements during my Ph.D period.

Besides, I would like to give my heartfelt thankfulness to my beloved family. Words cannot express my grateful to my mother, father and my fiancée, Miss Sheena Chen, for their sacrifice, firm support and sustained encouragements during the last four years of my Ph.D. This thesis would not be possible without the support and love from them.

Moreover, I want to thank the members in my research group for their support in my research, including Dr. Jian Liu, Dr. Hao Liu, Dr. Yan Jiao, Dr. Yao Zheng, Dr. Xin Du, Dr. Tianyi Ma, Dr. Sheng Chen, Mr. Ruifeng Zhou, Miss Jingjing Duan, Mr. Tianyu Yang, Mr. Jingrun Ran and Ms. Bita Bayatsarmadi, who have been currently or previously working in Prof. Qiao's research group in the University of Adelaide and/or University of Queensland.

Furthermore, I would like to thank Prof. Mietek Jaroniec and Dr. Denisa Hulicova-Jurkacova, for their valuable advices, comments and help during the design, preparation, composing and sharpening of my several research papers, without whose help it would be impossible to make them published on these top journals in my research fields. I would also like to give my thanks to Prof. Xi Wen Du and Miss Xue Min Chen in Tianjin University in China and Dr. Barry Wood in University of Queensland for their technique supports during my research.

Last but not least, I want to express my earnest appreciation to Australia Research Council Discovery Project which has finally supported my Ph.D research, China Scholarship Council who gave me the chance to study in Australia and covered the living costs during this period as well as the University of Adelaide and University of Queensland who top-upped the living allowance during my Ph.D.

Chapter 1 Literature Review

1.1 Introduction

This chapter reviews the application of carbon materials, especial the carbon nanomaterials, in the fields of energy storage and conversion, such as in a fuel cell, battery, supercapacitor or solar cell. The different types of carbon nanomaterials have been introduced from the aspect of their morphology, microstructure, synthesis and applicational performance. This chapter includes two sections: 1.2, carbon-based catalyst support in fuel cell applications; and 1.3, carbon materials and their energy conversion and storage applications.

1.2 Carbon-based catalyst support in fuel cell applications

This section is included in the thesis as it appears as a book chapter published by **J. Liang**, S. Z. Qiao, G. Q. Lu, D. Hulicova-Jurcakova, Carbon-based Catalyst Support in Fuel Cell Applications, in: J.M.D. Tascon, *Novel Carbon Adsorbents,* Elsevier Ltd, **2012**, 549.

It gives a review of the application of carbon materials as catalyst or catalyst support materials to be used in a fuel cell, both on the anode to catalyze the fuel oxidation reactions and on the cathode to catalyze the oxygen reduction reactions.

Statement of Authorship

Statement of Authorship

Title of Paper	Carbon-based Catalyst Support in Fuel Cell Applications
Publication Status	◉ Published, ○ Accepted for Publication, ○ Submitted for Publication, ○ Publication style
Publication Details	Novel Carbon Adsorbents, First Edition, Elsevier Ltd, 2012, 549–581 DOI: 10.1016/B978-0-08-097744-7.00018-1 ISBN: 9780080977447

Author Contributions

By signing the Statement of Authorship, each author certifies that their stated contribution to the publication is accurate and that permission is granted for the publication to be included in the candidate's thesis.

Name of Principal Author (Candidate)	Ji Liang (First Author)		
Contribution to the Paper	Manuscript composing		
Signature		Date	15/5/2014

Name of Co-Author	Prof. Shizhang Qiao		
Contribution to the Paper	Design of the project, organization of the research and supervision		
Signature		Date	15/5/2014

Name of Co-Author	Prof. Gao Qing Max Lu		
Contribution to the Paper	Manuscript revising		
Signature		Date	24/5/2014

Name of Co-Author	Dr. Denisa Hulicova-Jurcakova (Corresponding Author)		
Contribution to the Paper	Manuscript revising (The author is unable to response to the requirement of signing on this statement due to the physical conditions) My supervisor (Prof. Shizhang Qiao, the second author) will sign below on behalf of her.		
Signature		Date	15/5/2014

Liang, J., Qiao, S.Z., Lu, G.Q. & Hulicova-Jurcakova, D. (2012) Carbon-based catalyst support in fuel cell applications.
Novel Carbon Adsorbents, Elsevier pp. 549-581

1.3 Carbon-based catalyst support in fuel cell applications

This section is included in the thesis as it appears as a book chapter published by **J. Liang**, R. F. Zhou, D. Hulicova-Jurcakova and S. Z. Qiao, on Carbon Materials and Their Energy Conversion and Storage Applications, in: *Producing Fuels and Fine Chemicals from Biomass Using Nanomaterials*, Taylor & Francis Group, **2014**, 59.

It gives a review of the application of carbon materials as catalyst or catalyst support materials to be used in a variety of applications concerning the conversion and storage of energy, including fuel cells, batteries, supercapacitoers and solar cells.

Statement of Authorship

Statement of Authorship

Title of Paper	Carbon Materials and Their Energy Conversion and Storage Applications
Publication Status	◉ Published, ○ Accepted for Publication, ○ Submitted for Publication, ○ Publication style
Publication Details	Producing Fuel and Fine Chemicals from Biomass Using Nanomaterials CRC Press, 2013 Page 59-94 ISBN: 978-1-4665-5339-2 DOI: 10.1201/b15585-5

Author Contributions

By signing the Statement of Authorship, each author certifies that their stated contribution to the publication is accurate and that permission is granted for the publication to be included in the candidate's thesis.

Name of Principal Author (Candidate)	Ji Liang (First Author)		
Contribution to the Paper	Manuscript composing (60 %)		
Signature		Date	23/5/2014

Name of Co-Author	Ruifeng Zhou		
Contribution to the Paper	Manuscript composing (40 %)		
Signature		Date	23/5/2014

Name of Co-Author	Dr. Denisa Hulicova-Jurcakova		
Contribution to the Paper	Manuscript revising (The author is unable to response to the requirement of signing on this statement due to the physical conditions) My supervisor (Prof. Shizhang Qiao, the corresponding author) will sign below on behalf of her.		
Signature		Date	23/5/2014

Name of Co-Author	Prof. Shizhang Qiao		
Contribution to the Paper	Design of the project, organization of the research and supervision		
Signature		Date	23/5/2014

Liang, J., Zhou, R., Hulicova-Jurcakova, D. & Qiao, S.Z. (2013) Carbon materials and their energy conversion and storage applications.
Producing Fuel and Fine Chemicals from Biomass using Nanomaterials, CRC Press, pp. 59-94

Chapter 2 Graphitic Carbon Nitride and Carbon Composites for Oxygen Reduction

2.1 Introduction, Significance and Commentary

The state-of-the-art graphitic carbon nitride (g-C_3N_4) is a promising substitute for the expensive and vulnerable Pt catalyst for fuel cell cathode oxygen reduction reactions (ORR). It has also been investigated recently for other potential applications such as photocatalysis or hydrogen storage etc. Integration of this novel metal free catalyst on a suitable structured carbon substrate can bring about facile electron transfer, reduce the kinetic limitations and retain the structural stability. On this basis, we have for the first time designed and constructed a novel g-C_3N_4/Carbon with 3-dimensionally ordered macropores, which shows excellent ORR catalytic activity, extremely high fuel crossover tolerance and outstanding long term durability. To our knowledge, all these features have rarely been achieved in the case of other metal free catalysts, which make macroporous g-C_3N_4/Carbon catalyst promising for the next generation alkaline fuel cells based on organic fuels. The highlights in this work include:

1. We have for the first time designed and constructed a novel g-C_3N_4/Carbon with 3-dimensionally ordered macropores through a facile synthesis using very cheap cyanamide as a precursor and silica microspheres as hard template.

2. Macroporous g-C_3N_4/Carbon with the optimum 150 nm pore size shows much higher ORR catalytic performance than the mesoporous g-C_3N_4/C, which is closely comparable with commercial Pt/C in both reaction current and onset potential.

3. This catalyst possesses completely fuel poisoning tolerance, much superior to commercial Pt/C, and excellent long term durability in fuel cell environment, which is the highest among current g-C_3N_4/Carbons.

2.2 Facile Oxygen Reduction on a Three-Dimensionally Ordered Macroporous Graphitic C_3N_4/Carbon Composite Electrocatalyst

This section is included in the thesis as it appears as a research paper published by **J. Liang**, Y. Zheng, J. Chen, J. Liu, D. Hulicova-Jurcakova, M. Jaroniec and S. Z. Qiao, Facile Oxygen Reduction on a Three-Dimensionally Ordered Macroporous Graphitic C_3N_4/Carbon Composite Electrocatalyst. *Angew. Chem. Int. Ed.,* **2012**. *51*, 3892.

Statement of Authorship

Statement of Authorship

Title of Paper	Facile Oxygen Reduction on a Three-Dimensionally Ordered Macroporous Graphitic C3N4/Carbon Composite Electrocatalyst
Publication Status	◉ Published, ○ Accepted for Publication, ○ Submitted for Publication, ○ Publication style
Publication Details	Published on Angewandte Chemie International Edition (impact factor 13.734) Issue published online: 11 APR 2012 Article first published online: 2 MAR 2012 Manuscript Received: 13 NOV 2011 DOI: 10.1002/anie.201107981

Author Contributions

By signing the Statement of Authorship, each author certifies that their stated contribution to the publication is accurate and that permission is granted for the publication to be included in the candidate's thesis.

Name of Principal Author (Candidate)	Ji Liang (First Author)		
Contribution to the Paper	Research plan, material synthesis, most of the characterizations, performance assessment, manuscript drafting.		
Signature		Date	23/5/2014

Name of Co-Author	Dr. Yao Zheng		
Contribution to the Paper	Assistance with material synthesis, performance evaluation and part of characterization		
Signature		Date	23/5/2014

Name of Co-Author	Dr. Jun Chen		
Contribution to the Paper	Assistance with material performance evaluation		
Signature		Date	28/04/2014

Name of Co-Author	Dr. Denisa Hulicova-Jurcakova		
Contribution to the Paper	Manuscript revising (The author is unable to response to the requirement of signing on this statement due to the physical conditions) My supervisor (Prof. Shizhang Qiao, the second author) will sign below on behalf of her.		
Signature		Date	23/5/2014

Statement of Authorship

Title of Paper	Facile Oxygen Reduction on a Three-Dimensionally Ordered Macroporous Graphitic C3N4/Carbon Composite Electrocatalyst
Publication Status	◉ Published, ○ Accepted for Publication, ○ Submitted for Publication, ○ Publication style
Publication Details	Published on Angewandte Chemie International Edition (impact factor 13.734) Issue published online: 11 APR 2012 Article first published online: 2 MAR 2012 Manuscript Received: 13 NOV 2011 DOI: 10.1002/anie.201107981

Author Contributions

By signing the Statement of Authorship, each author certifies that their stated contribution to the publication is accurate and that permission is granted for the publication to be included in the candidate's thesis.

Name of Principal Author (Candidate)	Ji Liang		
Contribution to the Paper	Material synthesis, most of the characterizations, material performance assessment, manuscript drafting.		
Signature		Date	23/5/2014

Name of Co-Author	Dr. Jian Liu		
Contribution to the Paper	Assistance with manuscript revising and drafting		
Signature		Date	29/Apr/2014

Name of Co-Author	Prof. Mietek Jaroniec		
Contribution to the Paper	Assistance with manuscript revise and drafting		
Signature		Date	4/28/2014

Name of Co-Author	Prof. Shizhang Qiao		
Contribution to the Paper	Design of the project and structure of the manuscript, Organisation of the research and supervision Corresponding author, Assistance with manuscript revise and drafting		
Signature		Date	23/5/2014

Macroporous Catalysts

DOI: 10.1002/anie.201107981

Facile Oxygen Reduction on a Three-Dimensionally Ordered Macroporous Graphitic C_3N_4/Carbon Composite Electrocatalyst**

*Ji Liang, Yao Zheng, Jun Chen, Jian Liu, Denisa Hulicova-Jurcakova, Mietek Jaroniec, and Shi Zhang Qiao**

One of the greatest stumbling blocks hindering broad applications of fuel cells is the high cost and vulnerability of the platinum catalyst as well as the sluggish oxygen reduction reaction (ORR) on the cathode.[1] Although Pt alloys or non-noble metals have been developed as substitute catalysts for the ORR,[2,3] they still suffer from multiple disadvantages, such as low stability under fuel cell conditions, vulnerability to fuel crossover, and harmfulness to the environment.[4] Thus, the ongoing search for metal-free catalysts for the ORR has attracted much attention. In this regard, nitrogen-containing carbon materials are of particular interest owing to their catalytic activity towards the ORR brought about by nitrogen incorporation, which has been confirmed by both experimental studies[5–7] and quantum-mechanical calculations.[8] Among these materials, graphitic carbon nitride (g-C_3N_4) is especially promising because of its high nitrogen content, low cost, and easily tailorable structure,[9] which makes it potentially suitable for oxygen reduction as well as other applications, such as photocatalysis[10] or hydrogen storage, under mild conditions.[11]

However, the ORR electrocatalytic activity of g-C_3N_4 alone is still inferior to Pt catalysts.[12,13] This is because of the extremely low electrical conductivity (ca. 10^{-9} S m^{-1}[10,14]) of g-C_3N_4 as indicated by our recent theoretical calculations.[15] With the aim to better utilize this nitrogen-rich but poorly conducting material, a variety of carbon materials have been recently introduced into g-C_3N_4 by different routes, including mechanical mixing of g-C_3N_4 with carbon black[16] or in situ immobilization of g-C_3N_4 onto carbon black,[17] graphene,[13,18] or mesoporous carbon.[15] Compared to pristine g-C_3N_4, the aforementioned composites show better catalytic performance for ORR (that is, higher cathodic reaction current or lower ORR starting potential in a half-cell test). However, the effect of the structure of these composites on the catalytic properties is still unknown.

The porosity of catalyst in a fuel cell is critical for mass transport and access of the proton exchange ionomers.[19,20] However, the pores of previously investigated g-C_3N_4/carbon materials (g-C_3N_4/C) arise from pyrolysis of carbon precursors,[16,17] random stacking of graphene layers,[13,18] or mesoporous carbon with small pores.[15] The pore sizes of these composites are hard to control and often too narrow for efficient transport and access.[19,20] Furthermore, the potential prospects of g-C_3N_4/C as a substitute for Pt cannot be forecast on the basis of the current research because the ORR catalytic activity of the existing g-C_3N_4/C is hardly comparable to Pt[16–18] and/or they are not stable enough in the fuel cell environments.[13]

From this point of view, a more uniform structure with suitable pore size of the carbon substrate could be preferable for hybrid g-C_3N_4/C fuel cell catalysts. More specifically, a well-defined and continuous porous structure would facilitate reactant transport inside the pores, assure better contact between catalyst and ionomer, and better stability, as well as create an opportunity for an accurate evaluation of the structural effect of the added carbon on the ORR catalytic properties of g-C_3N_4/C. On this basis, a hard template method using silica microspheres as templates can be especially feasible and advantageous for preparing the carbon supports for g-C_3N_4 in several aspects. Preparation of g-C_3N_4/C with tunable pore size from meso to macropores could be easily achieved using this method.[21–27] Besides, the carbon materials thus synthesized feature uniform cage-like interconnected pores, which not only facilitate the mass transport but also avoid possible confusion in assessing the effect of pore sizes due to structural differences. Furthermore, this three-dimensionally interconnected structure would be stronger than the microscopically separated carbon materials, and the silica spheres are either commercially available or easy to fabricate, making the resulting g-C_3N_4/C potentially favorable for commercialization at low cost.

Herein we present the design and preparation of macroporous g-C_3N_4/C with three-dimensionally ordered interconnected structures using silica microspheres as hard templates. The main objective is to develop a high performance metal-free fuel cell catalyst, to evaluate the structural effect of the

[*] J. Liang, Y. Zheng, Dr. J. Liu, Dr. D. Hulicova-Jurcakova, Prof. S. Z. Qiao
ARC Centre of Excellence for Functional Nanomaterials
Australian Institute for Bioengineering and Nanotechnology
The University of Queensland, QLD 4072 (Australia)
E-mail: s.qiao@uq.edu.au
Prof. S. Z. Qiao
School of Chemical Engineering
The University of Adelaide, SA 5005 (Australia)
Dr. J. Chen
Intelligent Polymer Research Institute
ARC Centre of Excellence for Electromaterials Science
Australian Institute of Innovative Materials
University of Wollongong, NSW 2522 (Australia)
Prof. M. Jaroniec
Department of Chemistry and Biochemistry
Kent State University, Kent, OH 44242 (USA)

[**] This work is financially supported by the Australian Research Council (ARC) through the Discovery Project program (DP1095861, DP0987969).

Supporting information for this article is available on the WWW under http://dx.doi.org/10.1002/anie.201107981.

resulting g-C_3N_4/C on the electrocatalytic activity as well as to reveal its potential suitability as a substitute for Pt/C used in fuel cells. The catalytic activity of g-C_3N_4/C for ORR has been measured in comparison with mesoporous g-C_3N_4/C and commercial Pt/C. The g-C_3N_4/C catalysts with ordered pores of about 150 nm showed highest ORR performance, which was comparable with Pt/C in both the reaction current and the initial potential. Moreover, unlike the vulnerable commercial Pt/C, our material had extremely high tolerance against fuel crossover. Furthermore, this macroporous g-C_3N_4/C catalyst also possessed an excellent durability compared to both commercial Pt/C and previously reported g-C_3N_4/C in alkaline media.[13,18] To our knowledge, all of these properties have not been achieved in other metal-free catalysts, which make the current macroporous g-C_3N_4/C catalyst promising for the next generation of alkaline fuel cells based on organic fuels.

Macroporous g-C_3N_4/C was prepared as shown in Figure 1a. Silica spheres with different sizes were synthesized by

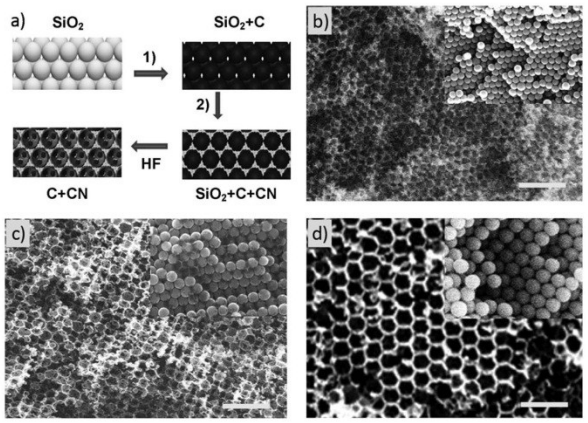

Figure 1. a) The synthesis of macroporous g-C_3N_4/C as a reversal of the SiO_2 sphere structure. Conditions: 1) Sucrose, 900 °C, N_2; 2) cyanamide, 550 °C, N_2. b)–d) Scanning electron microscopy (SEM) images of 150-C/CN, 230-C/CN, and 400-C/CN (and the corresponding silica spheres of each size (insets). Scale bars: 1 μm.

Stober's method[28] and packed up by gravitational sedimentation or solvent vaporization, forming an opal monolith. The monolith was then dried and calcined at 550 °C to obtain interconnected silica spheres. In the next step, a thin carbon shell was coated on the silica spheres (C@SiO_2) through sucrose infiltration followed by carbonization at 900 °C in nitrogen (Supporting Information, Figure S1). Afterward, melted cyanamide, as g-C_3N_4 precursor, was impregnated into the intersphere spaces of C@SiO_2, followed by heating at 550 °C in nitrogen to form g-C_3N_4/C@SiO_2. Finally, the silica template was removed with hydrofluoric acid after g-C_3N_4 synthesis, rather than in earlier stages, which successfully prevented the possible structural deterioration and pore blockage. Noticeably, as-synthesized g-C_3N_4/C (denoted as X-C/CN, where X is the pore size) has well-defined interconnected ordered macropores with the same size as the silica spheres (Figure 1).

The formation of g-C_3N_4 in the composite is confirmed by X-ray diffraction (XRD) on the basis of the peaks at 2θ located at 30° and 52° and corresponding to the (002) and the (101) face (Figure 2a).[9] The existence of g-C_3N_4 on carbon is

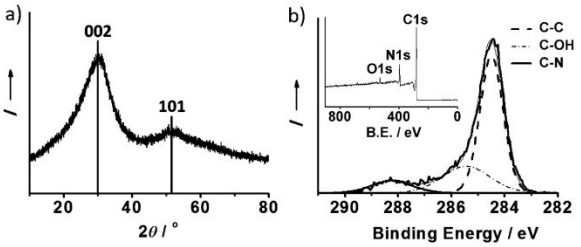

Figure 2. a) Typical XRD pattern obtained by Co Kα X-rays; b) typical high-resolution C1s XPS spectrum. Inset: corresponding survey scan of g-C_3N_4/C.

also evidenced by FTIR spectra on the basis of characteristic g-C_3N_4 absorbance peaks (Supporting Information, Figure S2). X-ray photoelectron spectroscopy (XPS) is another method to probe the integration of g-C_3N_4 with carbon. The survey scan spectrum of g-C_3N_4/C shows the presence of carbon, nitrogen, and oxygen (inset in Figure 2b). High resolution C1s spectra reveal the carbon status in the material (Figure 2b). The emergence of the peak at 288.3 eV corresponding to C–N coordination and the enhancement of the peak at 284.5 eV corresponding to C–C coordination, compared to pristine carbon and g-C_3N_4 (Supporting Information, Figure S3), confirm the successful incorporation of g-C_3N_4 onto carbon.[13,16] Another peak at 285.7 eV corresponds to C–OH, which is from the sucrose precursor and is commonly observed on carbon materials.[29] High-resolution scans of N1s in g-C_3N_4/C and g-C_3N_4 show similar nitrogen species, indicating comparable nitrogen status in both materials (Supporting Information, Figure S3). The porosity of these materials was investigated by nitrogen sorption measurements. As a result, all of the macroporous samples possess similar Brunauer–Emmett–Teller (BET) specific surface areas in the range between 50 and 100 $m^2 g^{-1}$; the surface area tends to decrease with increasing pore size (Supporting Information, Figure S5). No significant presence of mesopores or micropores was observed.

To further evaluate the pore size effect on the ORR catalytic activity of g-C_3N_4/C, mesoporous g-C_3N_4/C was also prepared for the purpose of comparison. The fabrication was firstly carried out by synthesizing mesoporous carbon using 12 nm colloidal silica spheres as a hard template as previously reported.[24] Cyanamide was then cast into the mesoporous carbon followed by heating at 550 °C, forming g-C_3N_4 inside mesoporous carbon (denoted as 12-C/CN). Both the 12-C/CN and the mesoporous carbon have the similar isotherm hysteresis loop confirming the presence of mesopores, but slight pore shrinkage is observed in 12-C/CN as compared to the parent carbon material (Supporting Information, Figure S6). These results indicate that both mesoporous materials possess similar cage like pores and g-C_3N_4 impregnation into mesoporous carbon does not significantly change its pore

structure. Transmission electron microscopy (TEM) observation also confirms the similar structures of mesoporous g-C_3N_4/C and carbon (Supporting Information, Figure S6). The uniform mesoporous structure of 12-C/CN is extremely suitable for comparison with its macroporous counterparts under study.

The ORR electrocatalytic activity of g-C_3N_4/C was firstly tested through conventional three-electrode cyclic voltammetry (CV) in O_2 or N_2 saturated 0.1 M KOH aqueous solutions (Figure 3a). A voltammogram without any significant peak was obtained in the absence of oxygen. The quasi-rectangular shape is due to a capacitor effect.[6,7] On the contrary, when oxygen was introduced, a characteristic ORR peak starting at −0.177 V was observed, showing the electrochemical reduction of oxygen initiated on g-C_3N_4/C. Compared to previous reports on nitrogen-doped carbon materials, the starting potential has increased positively,[6,30,31] indicating an easier ORR process on g-C_3N_4/C. At the same time, pure g-C_3N_4 with similar structure was also tested under the same conditions, showing the negligible ORR catalytic activity. The results indicate that the performance enhancement of g-C_3N_4/C was brought about by the introduction of carbon (Supporting Information, Figure S7).

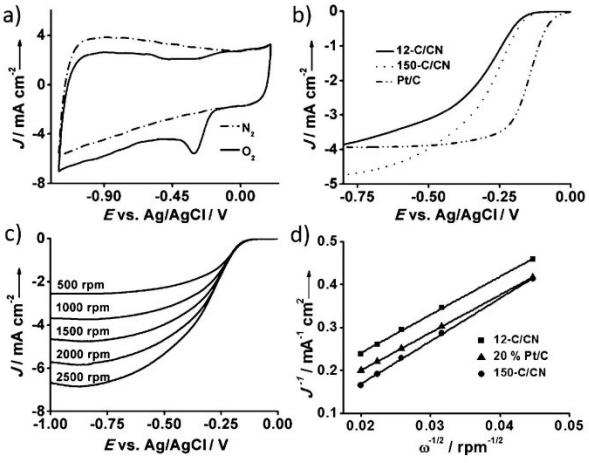

Figure 3. Catalytic activity towards electrochemical reduction of oxygen in 0.1 M KOH aqueous solution at room temperature. a) Cyclic voltammetry performed for 150-C/CN in O_2 and N_2; b) onset potential of mesoporous (12-C/CN), macroporous (150-C/CN) g-C_3N_4/C, and Pt/C obtained with a rotating disk electrode (RDE) at 1500 rpm and 5 mV s^{-1}; c) linear sweep voltammograms (LSVs) obtained for macroporous g-C_3N_4/C (150-C/CN) at various speeds; d) Koutecky–Levich plot for g-C_3N_4/C and Pt/C obtained from LSVs in (c) and the Supporting Information, Figure S7 at −0.6 V.

To further investigate the ORR catalytic activity of g-C_3N_4/C and the effect of pore size, these materials and commercial Pt/C (Vulcan, 20 wt %) were tested using a rotating disk electrode (RDE) in O_2-saturated 0.1 M KOH solution. The g-C_3N_4 amounts in each sample on the electrode in the RDE tests were the same by carefully controlling the catalyst ink concentration according to the elemental and thermogravimetric analysis results (Supporting Information, Figure S8 and Table S2). The ORR onset potentials of each sample were acquired from RDE linear sweep at 1500 rpm (Figure 3b). Remarkably, the macroporous g-C_3N_4/C showed obviously better performance than the mesoporous material in both onset potential (ca. −0.14 V) and reaction current density, which is comparable to Pt/C and indicates better performance brought about by larger pores.

Linear sweep voltammograms (LSV) were also recorded from 500 to 2500 rpm. LSVs for all g-C_3N_4/Cs show typical increasing current with higher rotations speeds (Figure 3c; Supporting Information, Figure S9). This result can be explained by shortened diffusion distance at high speeds, which is in accordance with other studies.[6,7] Noticeably, 12-C/CN showed a simultaneously increasing current density along with overpotential at all rotation speeds (Supporting Information, Figure S8), indicating a surface dominant reaction without a diffusion limited current, which is possibly due to the difficulties in reactant transfer within narrow 12 nm mesopores. The slight decrease in the current density at high rotation (2500 rpm) and high overpotential (> 0.9 V) might be caused by the fast O_2 consumption in the test cell.

The Koutecky–Levich plots (J^{-1} vs $\omega^{-1/2}$) of each catalyst are obtained from LSVs according to the current at −0.6 V, and all plots show good linearity at various rotation speeds (Figure 3d; Supporting Information, Figure S8). The macroporous samples exhibit higher current density than the mesoporous sample, and the 150-C/CN possesses the highest current density among all of the samples, which is even higher than that obtained for Pt/C at all rotation speeds (Figure 3b,d; Supporting Information, Figure S9), revealing the outstanding catalytic activity of this macroporous g-C_3N_4/C. The electron transfer numbers of ORR on different g-C_3N_4/C samples can be obtained from the slope of Koutecky–Levich plots (see details in the Supporting Information; these numbers are listed in Table S1).[32] All of the the g-C_3N_4/C samples possess a similar value of about 3, indicating a reasonably similar oxygen reduction process with combined two-electron and four-electron reaction pathways.[32]

To obtain insight into the ORR catalytic kinetic differences on g-C_3N_4/C with different pore sizes, the Tafel slopes, representing the overall resistance in the ORR process, were obtained according to the linear plots of LSVs at 1500 rpm for all g-C_3N_4/Cs (Figure 4a; Supporting Information, Figure S10). All of the plots show typical two-stage linear regions at low overpotential (> −0.2 V) and high overpotential (< −0.25 V), and the slope values are listed in Figure 4b.

In the low-overpotential region, where the overall ORR speed is determined by the surface reaction rate on the catalyst,[33] all of the Tafel slopes were between 51.1 and 72.6 mV dec^{-1}. The comparable values of the Tafel slopes for g-C_3N_4/C are also in agreement with their similar electron transfer numbers. This is in accordance with the fact that all g-C_3N_4/C can electrochemically reduce oxygen by a similar oxygen reduction process mechanism combining two- and four-electron reaction pathways. In the high overpotential region, where the overall ORR rate is dependent on the oxygen diffusion, the Tafel slope values for macroporous g-C_3N_4/Cs are between 150 and 190 mV dec^{-1}, which are much smaller than that of 12-C/CN (308 mV dec^{-1}), confirming

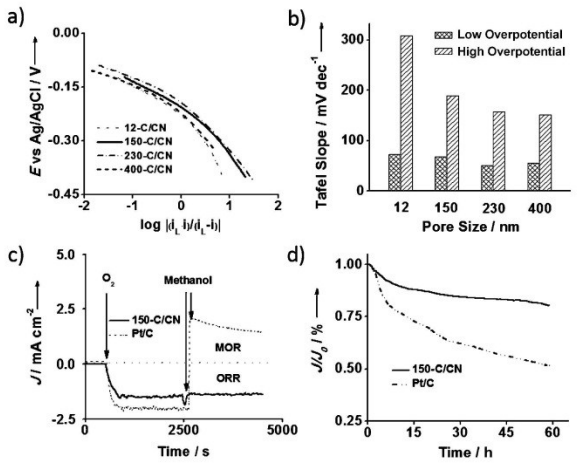

Figure 4. a) Tafel plots obtained from the RDE measurements on g-C_3N_4/C at 1500 rpm and b) the corresponding slope values of low and high overpotential regions; c) current–time chronoamperometric response of 150-C/CN and Pt/C in 0.1 M KOH solution. The arrow indicates the introduction of O_2 and 10 vol% methanol; d) current–time chronoamperometric response of 150-C/CN and Pt/C in O_2-saturated 0.1 M KOH solution.

significantly smoother reactant diffusion in the macropores than that in mesopores. As all of the samples show similar ORR mechanism at low overpotential, it is reasonable to assume that the better ORR activity of macroporous g-C_3N_4/C, compared to the mesoporous sample, is caused by the facile mass transfer in macropores. The superior performance of 150-C/CN could be the combination of both the positive effect of macropores on diffusion and the sufficient amount of active sites linked to the highest BET surface area among all macroporous samples.

For a new ORR electrocatalyst for fuel cells, a high catalytic selectivity for cathode reactions against fuel oxidation is important, especially when using small-molecule organic fuels, such as methanol, which could cross over through the polymer electrolyte membrane from anode to cathode, seriously compromising the whole cell performance.[13,31] The methanol crossover effect was evaluated on both macroporous g-C_3N_4/C and commercial Pt/C (Figure 4c). A negative current appeared when oxygen was introduced to N_2-saturated 0.1M KOH aqueous solution at about 500 s, indicating ORR occurred on both g-C_3N_4/C and Pt/C. After adding 10 vol% methanol to the electrolyte, g-C_3N_4/C retained stable current response whereas the current in the Pt/C system instantaneously jumped to positive values owing to the methanol oxidation reaction (MOR) on Pt/C. These results clearly show the excellent catalytic selectivity of g-C_3N_4/C and its better suitability as a cathode catalyst for direct methanol fuel cells than the vulnerable Pt/C.

The durability of g-C_3N_4/C and Pt/C was also assessed through chronoamperometric measurements at −0.3 V; at this potential the current was the largest, indicating the highest reaction rate (Figure 4d). The 100 h test only caused slight activity loss (reaction current decrease) on g-C_3N_4/C, whereas Pt/C lost nearly 50% of its initial activity in just 60 h, confirming a much better stability of active reaction sites on the g-C_3N_4/C materials than that on commercial Pt/C in alkaline environment, which is favored for the next generation alkaline fuel cells.

Taking into account the similar composition of the g-C_3N_4/C catalysts in this study and previous reports,[13] the observed enhancement in the ORR durability on the macroporous g-C_3N_4/C can be attributed to their uniquely porous structure. The composite catalyst synthesized in our study have a three-dimensionally interconnected porous structure, which effectively prevent the structural collapse or catalyst detachment that happens on microscopically separated carbon supported Pt or g-C_3N_4 catalysts, and thus help to keep our g-C_3N_4/C far more stable than other g-C_3N_4/C materials or commercial Pt/C.[13]

In summary, we have successfully designed and constructed a three-dimensionally ordered macroporous g-C_3N_4/C catalyst with outstanding ORR performance for fuel cells. This novel catalyst possesses prominent ORR catalytic activity, which is comparable with commercial Pt/C in both reaction current density and onset potential. As a metal-free catalyst, the macroporous g-C_3N_4/C showed much better fuel crossover resistance and long-term durability than the commercial Pt/C in alkaline medium. Furthermore, this material was synthesized through a simple procedure using inexpensive cyanamide as a precursor and easily fabricated silica microspheres as a template, which gives a great promise for large scale production. The pore size of g-C_3N_4/C can be easily tailored by using different size silica spheres as templates. All these features make macroporous g-C_3N_4/C a potentially promising and suitable substitute for the expensive noble metal catalysts in the next generation alkaline and direct methanol fuel cells.

Received: November 13, 2011
Published online: March 2, 2012

Keywords: carbon nitride · graphitic materials · heterogeneous catalysis · macroporous catalysts · oxygen reduction reaction

[1] B. C. H. Steele, A. Heinzel, *Nature* **2001**, *414*, 345.
[2] R. Bashyam, P. Zelenay, *Nature* **2006**, *443*, 63.
[3] H. Gasteiger, N. Markovi, *Science* **2009**, *324*, 48.
[4] D. S. Yu, E. Nagelli, F. Du, L. M. Dai, *J. Phys. Chem. Lett.* **2010**, *1*, 2165.
[5] K. Gong, F. Du, Z. Xia, M. Durstock, L. Dai, *Science* **2009**, *323*, 760.
[6] W. Yang, T.-P. Fellinger, M. Antonietti, *J. Am. Chem. Soc.* **2011**, *133*, 206.
[7] R. Liu, D. Wu, X. Feng, K. Müllen, *Angew. Chem.* **2010**, *122*, 2619; *Angew. Chem. Int. Ed.* **2010**, *49*, 2565.
[8] S. Maldonado, K. J. Stevenson, *J. Phys. Chem. B* **2005**, *109*, 4707.
[9] S. Hwang, S. Lee, J.-S. Yu, *Appl. Surf. Sci.* **2007**, *253*, 5656.
[10] X. Wang, K. Maeda, A. Thomas, K. Takanabe, G. Xin, J. M. Carlsson, K. Domen, M. Antonietti, *Nat. Mater.* **2009**, *8*, 76.
[11] S. S. Park, S. W. Chu, C. Xue, D. Zhao, C. S. Ha, *J. Mater. Chem.* **2011**, *21*, 10801.
[12] K. Kwon, Y. J. Sa, J. Y. Cheon, S. H. Joo, *Langmuir* **2012**, *28*, 991.

[13] S. Yang, X. Feng, X. Wang, K. Müllen, *Angew. Chem.* **2011**, *123*, 5451; *Angew. Chem. Int. Ed.* **2011**, *50*, 5339.
[14] Y. Zhang, T. Mori, J. Ye, M. Antonietti, *J. Am. Chem. Soc.* **2010**, *132*, 6294.
[15] Y. Zheng, Y. Jiao, J. Chen, J. Liu, J. Liang, A. Du, W. Zhang, Z. Zhu, S. Smith, M. Jaroniec, G. Q. M. Lu, S. Z. Qiao, *J. Am. Chem. Soc.* **2011**, *133*, 20116.
[16] S. M. Lyth, Y. Nabae, S. Moriya, S. Kuroki, M.-a. Kakimoto, J.-i. Ozaki, S. Miyata, *J. Phys. Chem. C* **2009**, *113*, 20148.
[17] S. M. Lyth, Y. Nabae, N. M. Islam, S. Kuroki, M. Kakimoto, S. Miyata, *J. Electroanal. Chem.* **2011**, *158*, B194.
[18] Y. Sun, C. Li, Y. Xu, H. Bai, Z. Yao, G. Shi, *Chem. Commun.* **2010**, *46*, 4740.
[19] E. Antolini, *Appl. Catal. B* **2009**, *88*, 1.
[20] H. Chang, S. H. Joo, C. Pak, *J. Mater. Chem.* **2007**, *17*, 3078.
[21] S. H. Joo, S. J. Choi, I. Oh, J. Kwak, Z. Liu, O. Terasaki, R. Ryoo, *Nature* **2001**, *412*, 169.
[22] A. Lu, A. Kiefer, W. Schmidt, F. Schuth, *Chem. Mater.* **2004**, *16*, 100.
[23] J. Fan, C. Yu, L. Wang, B. Tu, D. Zhao, Y. Sakamoto, O. Terasaki, *J. Am. Chem. Soc.* **2001**, *123*, 12113.
[24] H. I. Lee, G. D. Stucky, J. H. Kim, C. Pak, H. Chang, J. M. Kim, *Adv. Mater.* **2011**, *23*, 2357.
[25] Y. Meng, D. Gu, F. Zhang, Y. Shi, H. Yang, Z. Li, C. Yu, B. Tu, D. Zhao, *Angew. Chem.* **2005**, *117*, 7215; *Angew. Chem. Int. Ed.* **2005**, *44*, 7053.
[26] Y. Deng, T. Yu, Y. Wan, Y. Shi, Y. Meng, D. Gu, L. Zhang, Y. Huang, C. Liu, X. Wu, D. Zhao, *J. Am. Chem. Soc.* **2007**, *129*, 1690.
[27] C. Liang, S. Dai, *J. Am. Chem. Soc.* **2006**, *128*, 5316.
[28] W. Stober, A. Fink, E. Bohn, *J. Colloid Interface Sci.* **1968**, *26*, 62.
[29] H. Darmstadt, C. Roy, S. Kaliaguine, S. J. Choi, R. Ryoo, *Carbon* **2002**, *40*, 2673.
[30] S. H. Liu, J. R. Wu, *Int. J. Hydrogen Energy* **2011**, *36*, 87.
[31] L. Qu, Y. Liu, J. B. Baek, L. Dai, *ACS Nano* **2010**, *4*, 1321.
[32] H. S. Wroblowa, P. Yen Chi, G. Razumney, *J. Electroanal. Chem. Interfacial Electrochem.* **1976**, *69*, 195.
[33] M. T. de Groot, M. Merkx, A. H. Wonders, M. T. M. Koper, *J. Am. Chem. Soc.* **2005**, *127*, 7579.

2.3 Supplimentary Ingormation

This section is included in the thesis as as a supplimentary information to setion 2.2. It includes additional information which is not put in the main text of the published papr, but as an electronic supplimentary information freely accessed on-line.

Supporting Information

69451 Weinheim, Germany

Facile Oxygen Reduction on 3-Dimensionally Ordered Macroporous graphitic-C_3N_4/C Composite Electrocatalyst**

*Ji Liang, Yao Zheng, Jun Chen, Jian Liu, Denisa Hulicova-Jurcakova, Mietek Jaroniec, Shizhang Qiao**

Correspondence and requests for materials should be addressed to s.qiao@uq.edu.au (S.Z. Qiao)

Experimental Section:

1. Preparation of macroporous g-C_3N_4/Cs (pore size of 150-400 nm).

Silica spheres were prepared by Stober's method. In a typical synthesis of 150 nm silica, 250 ml of absolute ethanol was mixed with 19 ml of deionized water and 8 ml of 25 wt. % ammonia aqueous solution. The mixture was stirred vigorously for one hour followed by quick addition of 15 ml of tetraethylorthosilicate (TEOS). The solution was stirred for another 3 hours at 25 ºC; during this time the solution became milky white indicating the formation of silica spheres. Silica was separated by centrifugation at 20,000 rpm for 5 min, followed by 3 times washing with ethanol and 2 times with deionized water. The product was re-dispersed in 20 ml of ethanol and kept at 50 ºC in vacuum until all solvent vaporized. For the microspheres with larger particle sizes, they were packed up through gravimetrical sedimentation in aqueous suspension. The white solid was heated to 550 ºC with a ramp rate of 5 ºC min^{-1} and further calcined at 550 ºC in air for 5 h.

Sucrose was used as a carbon precursor. In a typical synthesis, 6.25 g of sucrose was dissolved in 25 ml aqueous solution containing 0.7 g of 98 wt. % sulfuric acid. Silica was immersed into sucrose solution of the same weight and kept in vacuum for 3 h at room temperature for thorough impregnation. Then the mixture was kept at 100 ºC for 6 h and 160 ºC for another 6 h for polymerization of sucrose. The solid was subsequently carbonized at 900 ºC in N_2 for 3 h to obtain carbon shell coated silica spheres (C@SiO_2).

The C@SiO_2 was lightly crashed and kept in melted cyanamide at 50 ºC for 3 h in vacuum. Then, the excess of cyanamide was removed and the black solid was heated at 550 ºC for 5.5 h with ramp rate of 4 ºC min^{-1} in N_2 to convert cyanamide into g-C_3N_4. The product was etched in excessive 20 wt. % hydrofluoric acid to remove the silica template. Macroporous g-C_3N_4 was also synthesized similarly by impregnating silica templates directly with cyanamide followed by heating and template removal.

2. Preparation of mesoporous g-C_3N_4/C

7 g of commercially available colloidal silica (Ludox HS 40, Aldrich, particle size 12 nm) was mixed with 50 g of deionized water, 0.3 g of 98 wt. % sulfuric acid and 3 g of sucrose. The mixture was stirred at 100 ºC until all the water vaporized. The resulted pitch-like solid was treated in the same way as described above for C@SiO_2.

Mesoporous carbon was obtained after the silica nanosperes were removed using hydrofluoric acid. The as prepared carbon has a BET surface area of ~1000 m^2 g^{-1} and pore volume of ~1.8 cm^3 g^{-1}. In the next step, 0.18 ml of melted cyanamide was mixed with 0.1 g of mesoporous carbon and kept at 50 ºC in vacuum for 3 h. The black powder was then heated to 550 ºC with a ramp rate of 4 ºC min^{-1} and kept at 550 ºC in N_2 for 5.5 h . The as prepared mesoporous g-C_3N_4/C has a BET surface area of ~500 m^2 g^{-1}.

3. Characterization

Silica particle size was in-situ monitored using a laser particle seizer (Zetasizer, Malvern). Nitrogen adsorption-desorption isotherms were measured on Tristar II (Micrometrics) at 77 K. Pore size distribution and specific surface area were obtained through Barrett-Joyner-Halenda (BJH) and Brunauer-Emmett-Teller (BET) methods from adsorption branch of the isotherm, at a relative pressure range of $P/P_0 = 0.05\text{-}0.25$.

The phase crystallinity and d-spacing were determined through X-ray diffraction with Co Kα radiation (Miniflex, Rigaku). FTIR was conducted on Nicolet 6700 FT-IR instrument. XPS analysis was carried out on Kratos Axis Ultra XPS instrument with a hemispherical 165 mm electron energy analyzer. Microstructures of the samples were observed on TEM (JEM-1010, JEOL) and SEM (JSM-6300 F, JEOL).

g-C_3N_4 content of each sample was determined on an elemental analyzer through V_2O_5 enhanced combustion at 1020 ºC (NA 1500 Elemental Analyser, Carlo Erba). Duplicated test was done to minimize incidental errors. Thermogravimetric Analysis (TGA) was conducted on TGA/DTA system (STAR^e, Mettler Toledo) at 25-750 ºC using a 15 ml min^{-1} N_2 flow.

4. Electrode preparation and electrochemical test

g-C_3N_4/C samples with different pore sizes were carefully weighted according to the elemental analysis results (Table S 1) in order to get the same g-C_3N_4 content. The samples were then dispersed in deionized water (18.2 MΩ) and g-C_3N_4 concentration was controlled to be 0.6 mg/ml. The mixture was ultrasonicated for 10 min to obtain a homogenous catalyst ink.

To prepare the working electrode for CV measurements, 20 µl of ink was dipped on a mirror polished glass carbon electrode (diameter of 3 mm). The electrode was dried in air, and another 5 µl of 1 % Nafion aqueous solution was covered on the electrode surface. After drying at 50 ºC, the working electrode was inserted into the cell setup, which composed of a platinum counter electrode, an Ag/AgCl reference electrode and a 20 ml glass cell containing 15 ml of 0.1 M KOH aqueous solution. The whole setup was sealed by o-ring, with two tubes for O_2/N_2 supply and tail gas outlet.

CV experiments were performed on Solartron electrochemical analysis station. Before test, a 4 ml/min O_2/N_2 flow was used through the electrolyte in the cell for 20 min to saturate it with O_2/N_2. The cell was kept at 25 ºC in the test for all samples. The test was performed from 0.2 V to -1.2 V versus Ag/AgCl/NaCl (3 M), with sweep rate of 100 mV s^{-1}. The sample was tested for 3 times to avoid any incidental errors. Long term durability test of 150-C/CN and Pt/C (Vulcan, 20 wt. %) was also conducted using the same setup as in CV. The test was performed for 100 h for g-C_3N_4/C and 60 h for Pt/C with 4 ml min^{-1} O_2 continuous flow at 25 ºC.

For the RDE test, catalyst inks were prepared by ultrasonically dispersing the catalysts in water using g-C_3N_4 concentration of 0.6 mg ml^{-1}. A rotating glass carbon electrode (0.2826 cm^2, Princeton

Applied Research, USA) was used as a substrate for the catalyst and the modified RDE was prepared as reported elsewhere [1]. Specifically, a total of 40 μL ink (24 μg g-C_3N_4) was pipetted onto the electrode. After drying this amount corresponded to the g-C_3N_4 loading of 85 μg cm^{-2}; 10 μl of Nafion solution (0.1 wt % in water) was then dropped on the electrode to ensure the attachment of the g-C_3N_4/C on the substrate. The modified-glass carbon electrode was dried in air to let the solvents evaporate completely.

Electrochemical measurements were carried out using a 636 rotation disk electrode (RDE, Princeton Applied Research, USA) controlled with a CHI 720c electrochemical Biopotentiostat (CH Instruments, USA) under ambient conditions. A Pt mesh and an Ag/AgCl (3 M NaCl) were used as the counter and reference electrodes, respectively. The linear sweep voltammograms of the modified glass carbon electrode were recorded in O_2 saturated 0.1 M KOH with a scan rate of 5 mV s^{-1} at various rotating speeds from 500 to 2500 rpm. After each scan, the electrolyte was saturated with O_2 again for 5 minutes.

The Koutecky-Levich plots were obtained by linear fitting of the reciprocal rotating speed versus reciprocal current density collected at -0.6 V. The electron transfer numbers involved in a typical ORR process can be calculated from the slopes of Koutecky-Levich equation as follows:

$$B=0.2\ nFA\nu^{-1/6}C_{O2}D_{O2}^{2/3}$$

where n is the number of electrons transferred per oxygen molecule, F is the Faraday constant （96485 C mol^{-1}）, D_{O2} is the diffusion coefficient of O_2 in 0.1 M KOH (1.9×10^{-5} cm s^{-1}), ν is the kinetic viscosity, and C_{O2} is the concentration of O_2 (1.2×10^{-3} mol L^{-1}). The constant 0.2 is adopted when the rotating speed is in rpm. The electron transfer numbers as calculated are listed in Table S1

Table S1 Electron transfer numbers on g-C_3N_4/C

Sample Name	**12-C/CN**	**150-C/CN**	**230-C/CN**	**400-C/CN**
Electron Transfer Numbers	3.17	2.89	3.06	3.12

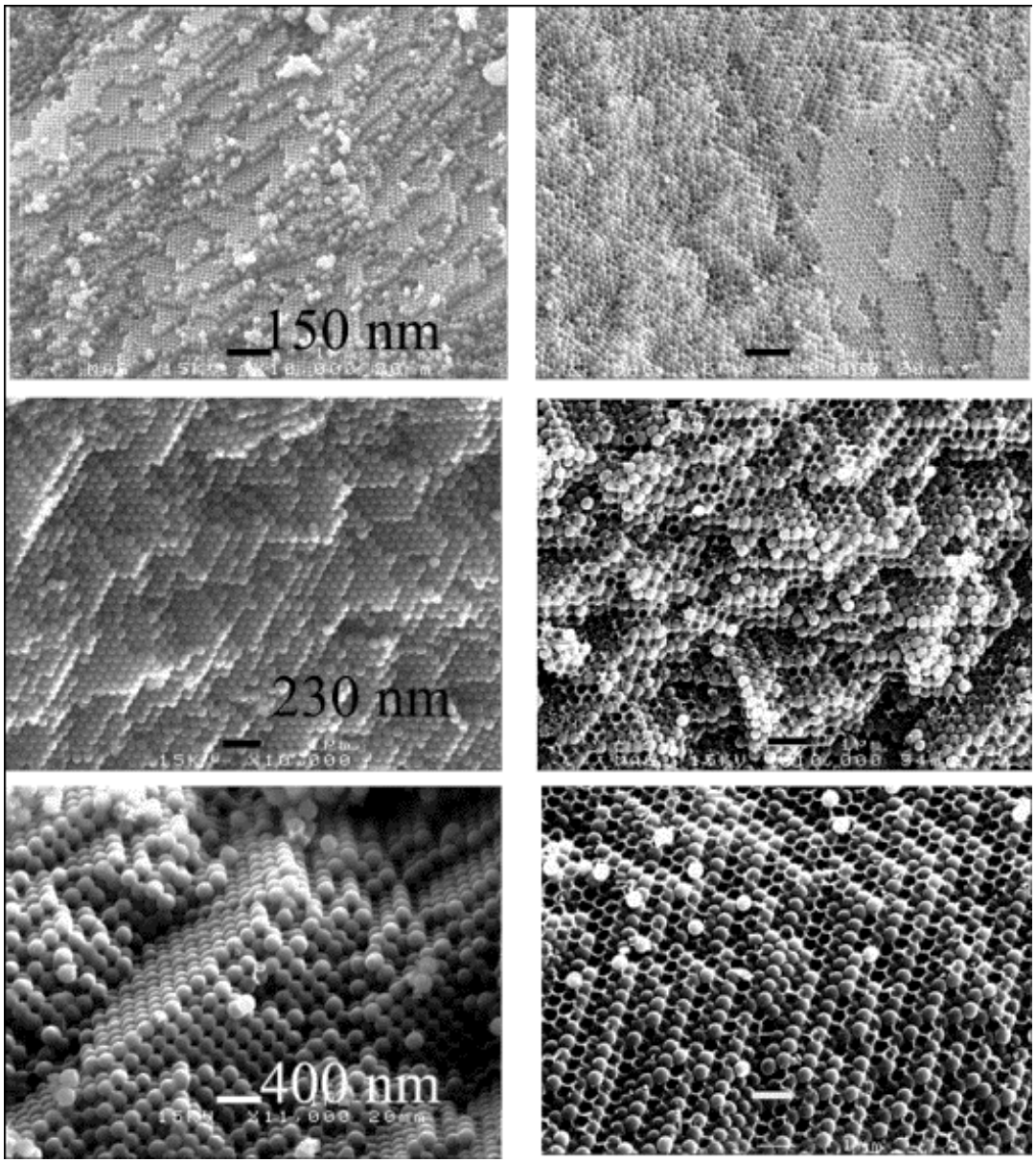

Figure S1 SEM images of $C@SiO_2$ spheres and g-C_3N_4/$C@SiO_2$ (from left to right) with different pore sizes from 150 nm to 400 nm (from top to bottom). All images are with scale bar of 1 micron.

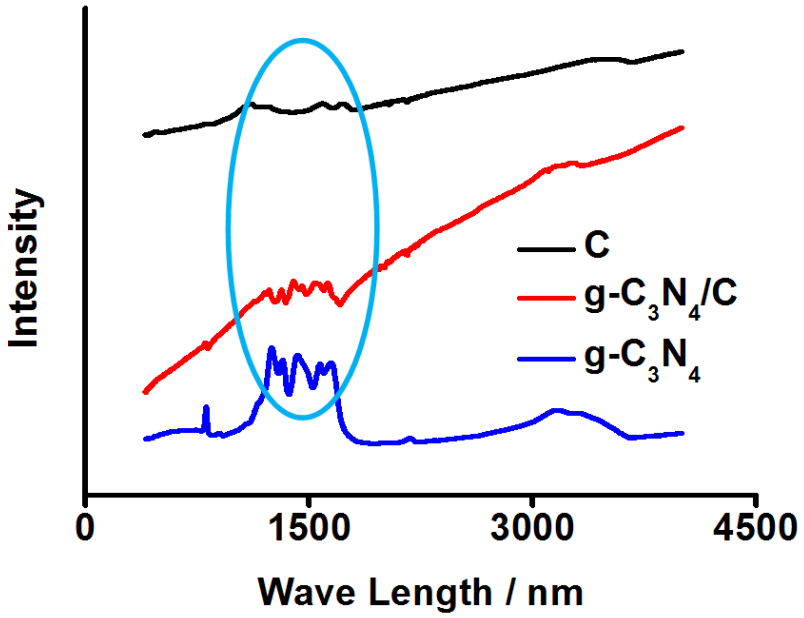

Figure S2. Fourier transform infrared spectroscopy of C, g-C_3N_4/C and pure g-C_3N_4. The g-C_3N_4/C showed characteristic peaks that appeared in pure g-C_3N_4, indicating the existence of g-C_3N_4 on carbon.

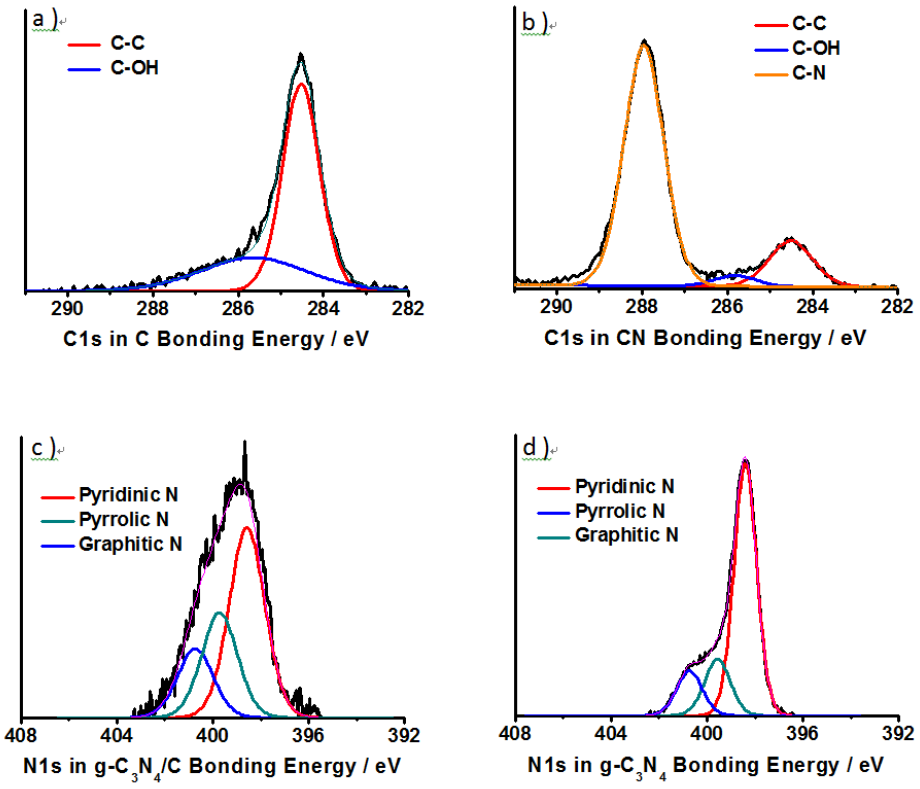

Figure S3. High resolution C1s XPS spectra of a) pristine carbon and b) g-C_3N_4; c, d) N1s spectra of 150-C/CN and pristine g-C_3N_4, showing typical pyridinic N, pyrrolic N and graphitic N; all the spectra are base-line subtracted.

Noticeably, a peak centered at ~284.5 eV was observed in b) C1s spectra of pristine g-C_3N_4, which is commonly believed as the response of C=C bond. However, it is highly unlikely to be such sp^2 environment in carbon nitride because carbon atoms are bonded with three nitrogen atoms in the graphite-like atom layers of stoichiometric g-C_3N_4. Similar feature was also observed in other published researches using different precursors to synthesize g-C_3N_4 [2, 3]. The reason for this is not very clear so far. To avoid any carbon contamination which would bring about this peak, thermal gravimetric analysis (TGA) was conducted on pristine g-C_3N_4 and carbon in nitrogen atmosphere as shown in Figure S4, and the sample completely decomposed before 750 ºC in N_2 i.e. 100 % weight loss, at which condition carbon is stable and the weight loss is negligible. The presence of this peak might be the result of C-N=C bond within sp^2 environment, but further study is needed.

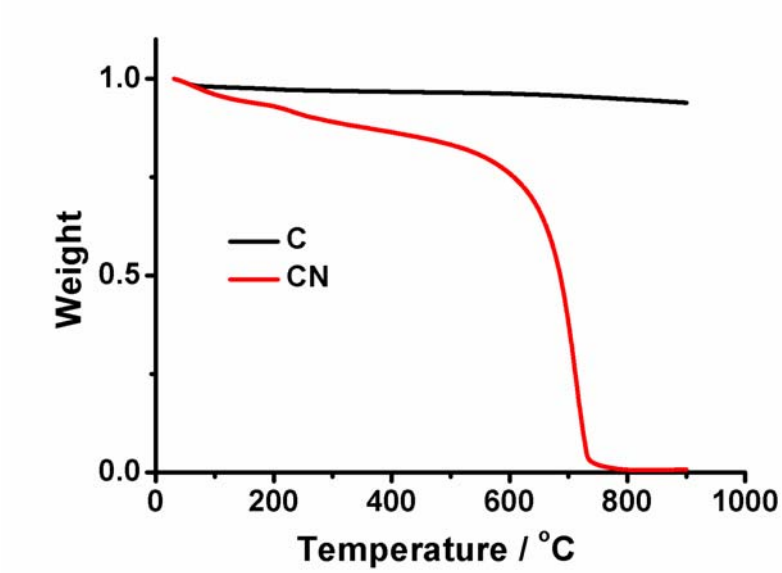

Figure S4. TGA weight lose curve of carbon and g-C_3N_4 tested in N_2 with ramp rate of 5 ºC/min. Pristine g-C_3N_4 subjected to a total weight loss before 750 ºC while carbon showed no obvious weight loss, indicating no carbon contamination in carbon nitride. The aforementioned C-C response in the XPS spectra in carbon nitride is not caused by carbon impurities.

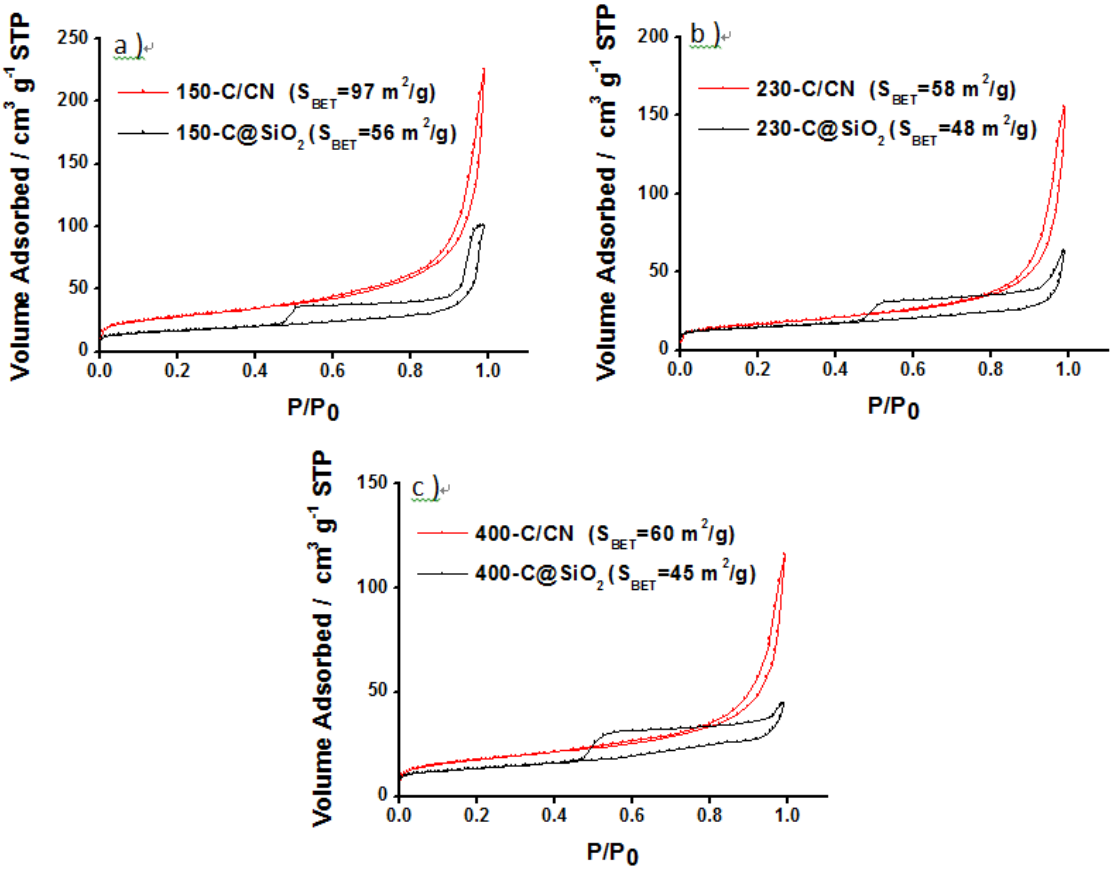

Figure S5. Nitrogen adsorption-desorption isotherms of macroporous g-C_3N_4/C and corresponding C@SiO_2 parent templates. Specific surface areas of each sample are also listed.

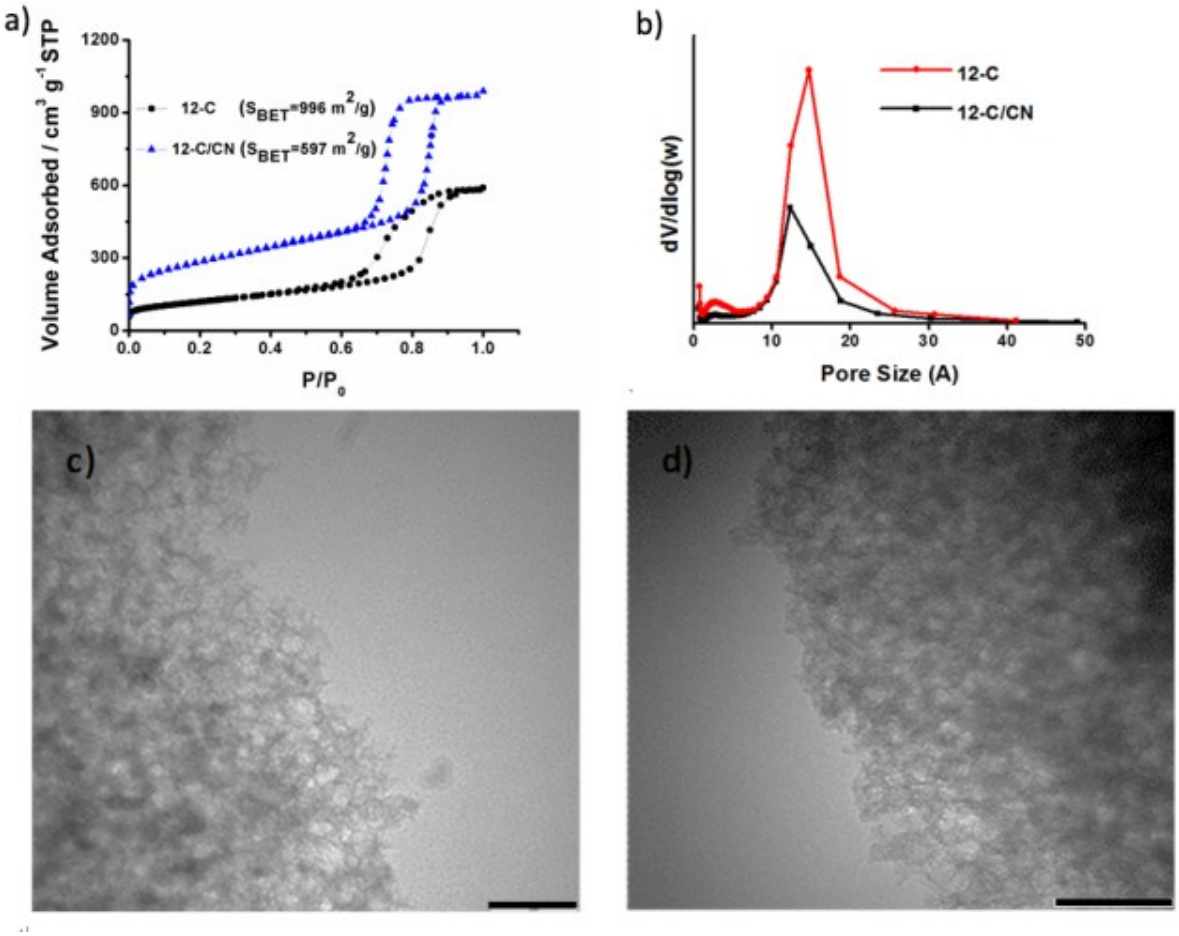

Figure S6. Nitrogen adsorption and desorption isotherms (a) and pore size distribution (b) of the mesoporous 12-C and 12-C/CN samples; TEM images of 12-C (c) and 12-C/CN (d), the scale bar is 50 nm.

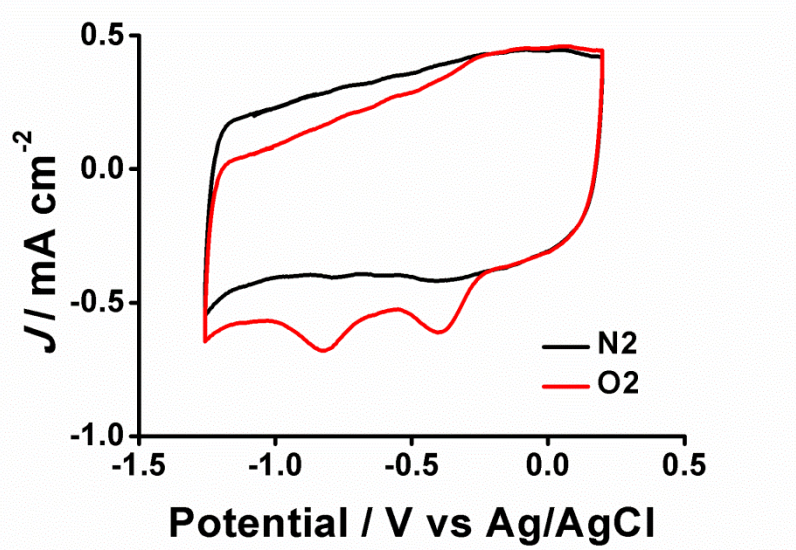

Figure S7 CV test results on pure g-C3N4 without carbon incorporation in 0.1 M KOH aqueous solution with N_2 or O_2 saturated.

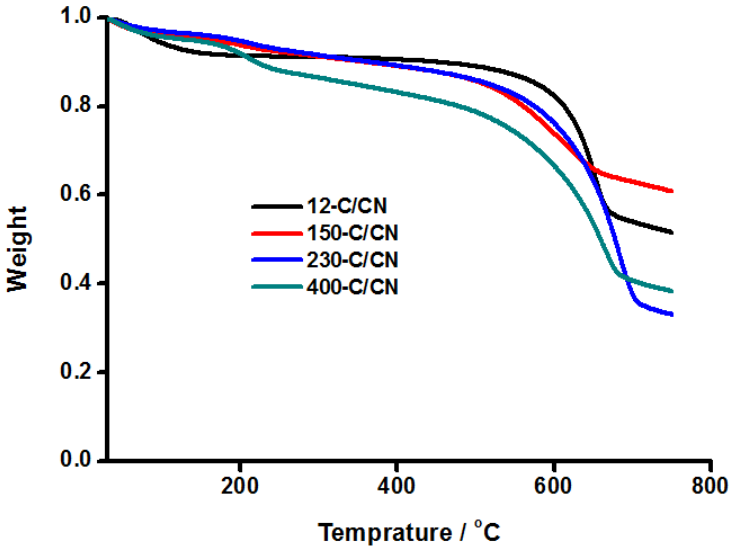

Figure S8. TGA weight change curves of g-C_3N_4/C tested in N_2 with a ramp rate of 5 ºC/min.

Table S2 Elemental compositions of the samples obtained from TGA and elemental analysis.*

Sample Name	12-C/CN	150-C/CN	230-C/CN	400-C/CN
C wt. %	67.69	67.75	49.83	35.13
N wt. %	28.22	21.03	37.82	25.60
H wt. %	0.97	1.83	1.73	9.27
CN wt. % by EA	44.20	32.83	60.19	60.09
CN wt. % by TGA	43.84	34.26	63.11	57.90

*Elemental analysis (EA) and thermogravimetric analysis (TGA) results of each sample, and the corresponding g-C_3N_4 content were calculated assuming that C:N in g-C_3N_4 is 3:4 and H forms H_2O. Duplicated EA was conducted by combustion in oxygen with the assistance of V_2O_5 and showed very close results.

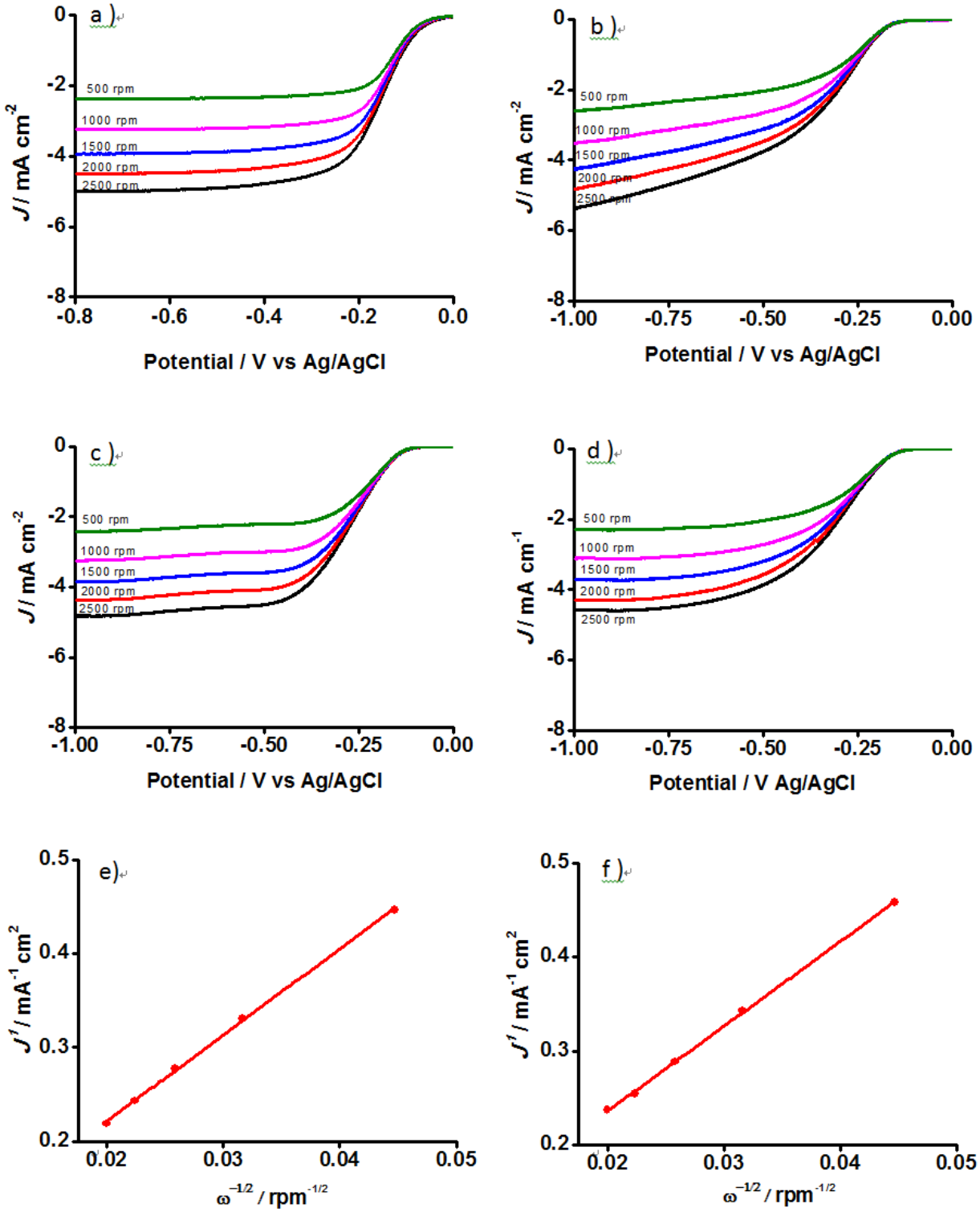

Figure S9. LSVs of a) Pt/C, b) 12-C/CN, c) 230-C/CN, d) 400-C/CN at different rotation speeds (from 500 to 2500 rpm); e) and f) Koutecky-Levich plots for 230-C/CN and 400-C/CN at -0.6 V.

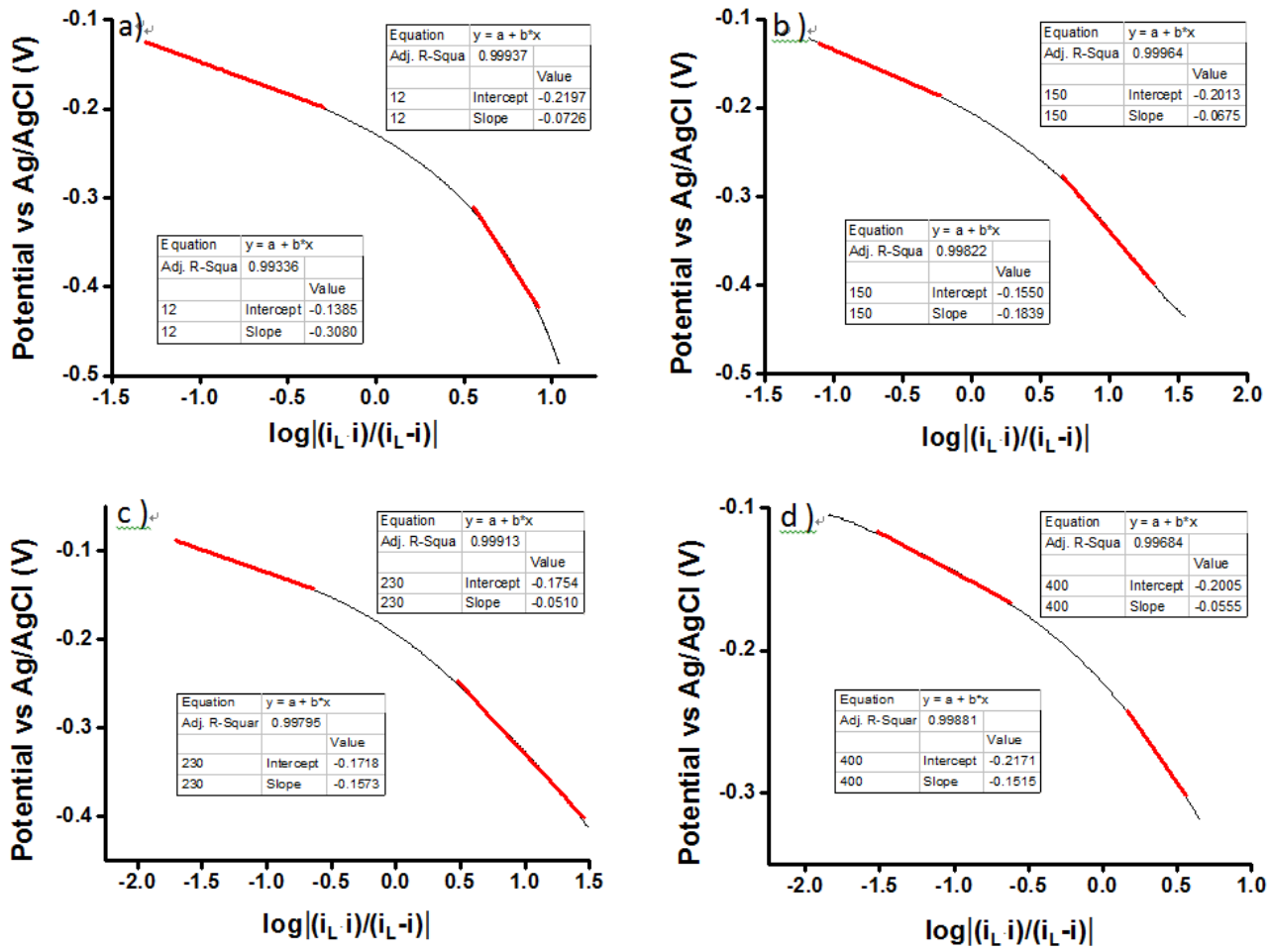

Figure S10. Linear fitting of Tafel plots at low and high over potentials regions of a) 12-C/CN, b) 150-C/CN, c) 230-C/CN and d) 400-C/CN. All the fittings are with adjusted R square larger than 0.99, showing the good linearity and fitness.

References

[1] U. A. Paulus, T. J. Schmidt, H. A. Gasteiger, R. J. Behm, *Journal of Electroanalytical Chemistry* **2001**, *495*, 134.

[2] Q. Guo, Y. Xie, X. Wang, S. Lv, T. Hou, X. Liu, *Chemical Physics Letters* **2003**, *380*, 84.

[3] H. Yan, Y. Chen, S. Xu, *International Journal of Hydrogen Energy* In press, corrected proof.

Chapter 3 N-doped Carbon Hybrids with Synergistically Enhanced Performance for ORR

3.1 Introduction, Significance and Commentary

The design and synthesis of advanced porous carbon materials with high surface area, accessible porosity and good conductivity for various applications such as electrochemistry, adsorption, separation and catalysis are extremely desirable but greatly challenging. In this work, we have designed and prepared a new hybrid carbon material composed of hierarchical ordered porous carbon and in-situ grown graphene, which has successfully combined the above mentioned merits of the advanced carbon materials and resulted in an excellent and synergistically enhanced electrochemical catalysis performances.

The highlights and novelty in this work include:

1. Novel Structure
   a). We have for the first time designed and synthesized a novel N-doped hybrid carbon material through a bottom-up route. The prepared material is composed of hierarchical porous carbon micro blocks interlinked with in-situ grown graphene. To the best of our knowledge, this is the first study to natively grow graphene from porous carbon.
   b). Large surface area, high accessibility and excellent electron conductivity have been successfully achieved by integrating the ordered mesopores, 3D interconnected & ordered macropores and in-situ formed bridging graphene on this material.
2. New Method & Interesting Mechanism
   a). The hierarchical porosity with large surface area of this carbon material has been for the first time achieved by using polystyrene spheres as hard templates for 3D macropores and F127 as a soft template for 2D mesopores. No harsh treatments or hazardous chemicals, as in many previous studies for similar structure, are required to remove these templates (eg. hydrofluoric acid to etch the silica/alumina templates). The preparation is convenient, economical, eco-friendly and practically ready for mass-production.
   b). This hybrid material was synthesized by one-step heating of hierarchical porous resin and melamine/g-C3N4 via a very interesting mechanism: the resin acted as a precursor for both porous carbon and graphene; the melamine served as the template to direct the formation of graphene on porous carbon and initial N precursor to dope this graphene/carbon hybrid at low temperature (<550 °C); while the g-C3N4 further doped N on this hybrid and also prevented N leaching from it at higher temperature.
3. High Performance
   a). It is found that this carbon material show an excellent ORR catalytic performance with synergistically enhanced activity compared with the analogues, considering both its positive

onset potential and high reaction current. Tafel analysis confirms that the good performance was brought from its unique structural advantages.

b). This completely metal-free material has also shown a complete methanol tolerance and excellent long-term stability, which is much superior to the commercial Pt/C and makes our porous carbon material potentially suitable for applications such as fuel cells and batteries.

3.2 N-Doped Graphene Natively Grown on Hierarchical Ordered Porous Carbon for Enhanced Oxygen Reduction

This section is included in the thesis as it appears as a front inside cover paper published by **J. Liang**, X. Du, C. Gibson, X. W. Du and S. Z. Qiao. A Hybrid of Nitrogen-Doped Graphene and Hierarchical Porous Carbon for Enhanced Oxygen Reduction, *Adv. Mater.*, **2013**, *25*, 6226.

Statement of Authorship

Statement of Authorship

Title of Paper	N-Doped Graphene Natively Grown on Hierarchical Ordered Porous Carbon for Enhanced Oxygen Reduction
Publication Status	◉ Published, ○ Accepted for Publication, ○ Submitted for Publication, ○ Publication style
Publication Details	Article published by Advanced Materials (Front Inside Cover, impact factor 14.829) Article first published online: 20 AUG 2013 DOI: 10.1002/adma.201302569

Author Contributions

By signing the Statement of Authorship, each author certifies that their stated contribution to the publication is accurate and that permission is granted for the publication to be included in the candidate's thesis.

Name of Principal Author (Candidate)	Ji Liang (First Author)		
Contribution to the Paper	Research plan, material synthesis, most of the characterizations, material performance assessment, manuscript drafting.		
Signature		Date	23/5/2014

Name of Co-Author	Dr. Xin Du		
Contribution to the Paper	Assistance with material synthesis and part of characterization		
Signature		Date	Apr. 28, 2014

Name of Co-Author	Dr. Christopher Gibson		
Contribution to the Paper	Assistance with key material characterization (atom force microscopy)		
Signature		Date	29-4-2014

Name of Co-Author	Prof. Xi Wen Du		
Contribution to the Paper	Assistance with key material characterization (transmission electron microscopy and elemental mapping)		
Signature		Date	23/5/2014

Statement of Authorship

Title of Paper	N-Doped Graphene Natively Grown on Hierarchical Ordered Porous Carbon for Enhanced Oxygen Reduction
Publication Status	◉ Published, ○ Accepted for Publication, ○ Submitted for Publication, ○ Publication style
Publication Details	Article first published online: 20 AUG 2013 DOI: 10.1002/adma.201302569

Author Contributions

By signing the Statement of Authorship, each author certifies that their stated contribution to the publication is accurate and that permission is granted for the publication to be included in the candidate's thesis.

Name of Principal Author (Candidate)	Ji Liang (First Author)		
Contribution to the Paper	Research plan, material synthesis, most of the characterizations, material performance assessment, manuscript drafting.		
Signature		Date	23/5/2014

Name of Co-Author	Prof. Shizhang Qiao		
Contribution to the Paper	Design of the project, organisation of the research and supervision Corresponding Author, help with manuscript revise and drafting		
Signature		Date	23/5/2014

Name of Co-Author			
Contribution to the Paper			
Signature		Date	

Name of Co-Author			
Contribution to the Paper			
Signature		Date	

Vol. 25 • No. 43 • November 20 • 2013

D10488

www.advmat.de

ADVANCED MATERIALS

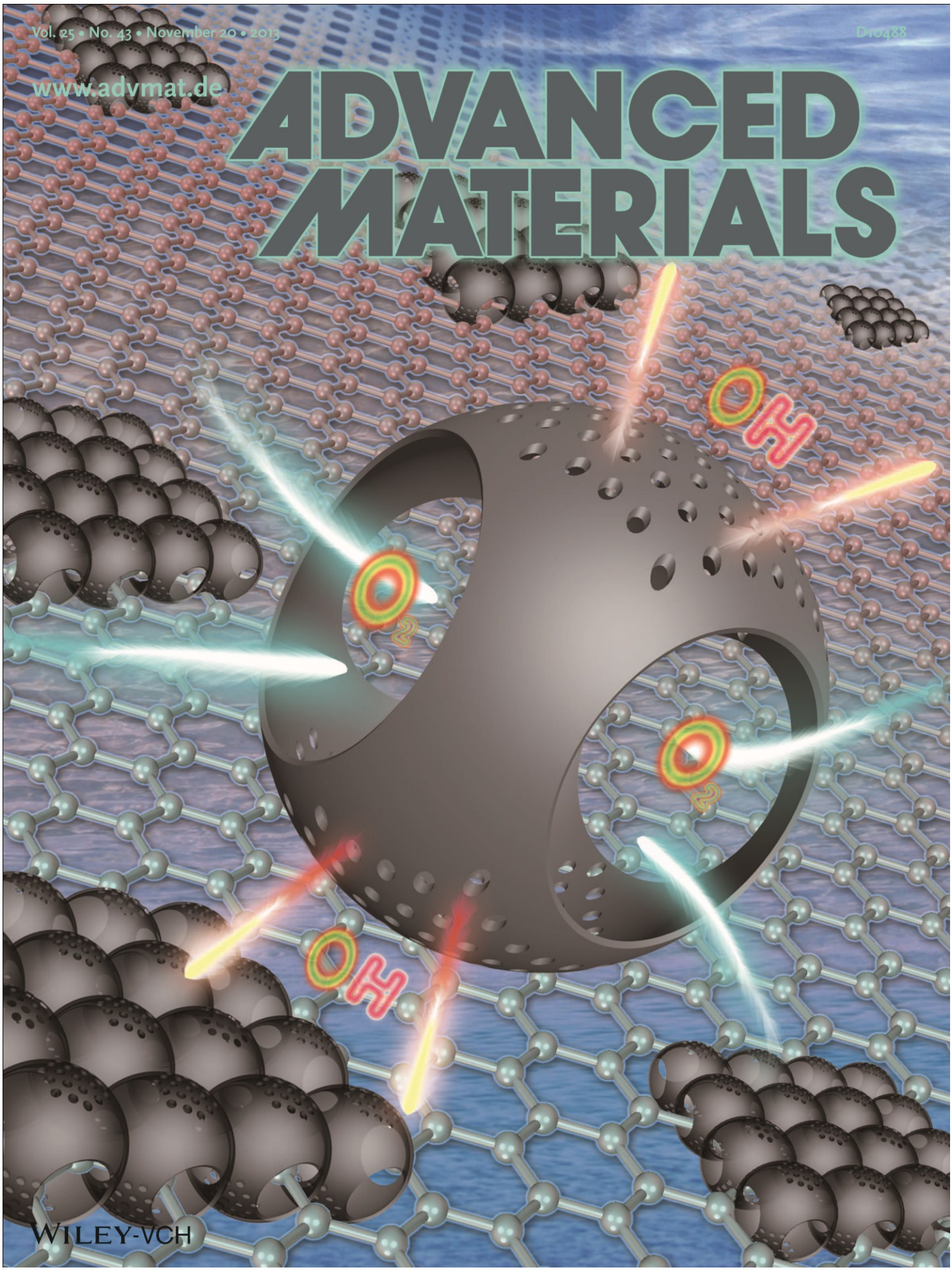

WILEY-VCH

ADVANCED MATERIALS
www.advmat.de

Materials Views
www.MaterialsViews.com

N-Doped Graphene Natively Grown on Hierarchical Ordered Porous Carbon for Enhanced Oxygen Reduction

*Ji Liang, Xin Du, Christopher Gibson, Xi Wen Du, and Shi Zhang Qiao**

Highly porous carbon materials with tunable pore sizes have been widely employed in phase separation, gas adsorption, catalysis and organic conversion.[1–6] Among them, the mesoporous carbon is especially popular and important in the applications of electrochemical energy storage and conversion due to its unique structural features which can offer both high surface area for large amounts of potential active sites and channels for reactant/product transfer, respectively.[7,8] However, in the processes requiring fast mass exchanges such as oxygen reduction reactions (ORR), these mesopores seem incapable of providing a reactant/product transfer that is smooth enough to maintain the swift electrochemical reactions. In our previous studies, by simply enlarging the 3-dimensional (3D) pores in a carbon based catalyst from meso-size (12 nm) to macro-size (150 nm), its ORR catalytic performance could be remarkably enhanced due to a facilitated mass transfer in the macropores.[9] However, the relatively low surface area in this macroporous material may lead to a smaller number of exposed active sites. To tackle the issue of high surface and high accessibility in carbons with uniform pore sizes, hierarchical porous carbons with well-defined mesopores located at the walls of the macropores have been recently developed. They provide both large surface area for active site exposure on the mesopores and efficient mass transfer through macropores.[10,11] Similar to many other porous materials, such highly porous carbon could suffer from a low crystalline degree and numerous defects, which would consequently result in poor electron conductivity and inevitably compromise the electrochemical catalytic activity.[12,13] Furthermore, in most of the fabrications, silica materials have been frequently employed as sacrificial templates, which always need to be removed under extremely harsh and hazardous conditions, making these porous carbons expensive and risky for large scale production.[10,11]

J. Liang, Dr. X. Du, Prof. S. Z. Qiao
School of Chemical Engineering
the University of Adelaide
Adelaide, SA 5005, Australia
E-mail: s.qiao@adelaide.edu.au
Dr. C. Gibson
Centre for Nanoscale Science and Technology
School of Chemical and Physical Sciences
Flinders University
Adelaide, SA 5043, Australia
Prof. X. W. Du
School of Materials Science and Engineering
Tianjin University
Tianjin, 300072, China

DOI: 10.1002/adma.201302569

Graphene, the 2-dimensional (2D) nanosheets composed of few layers of sp^2–hybridized carbon atoms, has also been widely studied as a candidate for electrochemical applications in fuel cells, metal-air batteries and sensors etc., particularly because of its excellent electrical properties and theoretically ultrahigh specific surface area, which is greatly important and desirable for electrochemical processes.[7,14–19] To facilitate its mass transportation, various pores have been introduced into graphene by modifications such as: employing spacers like in-situ grown[20] or post grafted[21] carbon nanotubes, removable hard templates,[22–24] sacrificial surfactants,[25] or various nanoparticles,[26,27] as well as complicated physical treatments such as cyro-drying[28,29] to form "out-of-plane" meso/macropores between the graphene nanosheets; using graphitic carbon nitride ($g\text{-}C_3N_4$) as a sacrificial template[23,24] or treating graphene with strong chemical activation agents[30,31] to produce irregular "in-plane" pores on the graphene nanosheets. However, in most of these processes, the graphene with "out-of-plane" pores suffers from unexpectedly low specific surface areas due to the re-stacking of the nanosheets with large aspect ratio, making them less competitive because of the potentially less active sites for catalysis; whilst the hazardous procedure and/or the low yield of the approaches to form "in-plane" pores render the materials environmentally and economically unfavorable. Moreover, the high mechanical flexibility of graphene as well as the loose contact between these nanosheets also leads to the suspicion of structural instability of the porosity in above mentioned materials.

With the aim of architecting a material with high surface area, stable hierarchical structures, and good conductivity by an economical and low-hazardous approach, we report here for the first time an elaborate bottom-up design and successful preparation of a nitrogen-doped hybrid carbon material, which is composed of hierarchical porous carbon micro blocks interconnected with in-situ grown graphene. Remarkably, the excellent structural properties, such as large surface area, high accessibility, and good conductivity render this metal-free material a very suitable candidate for electrochemical applications, which is approved by its inherent ORR catalytic actives with synergistically enhanced performance.

The nitrogen-doped ordered macro-mesoporous carbon/graphene (N-OMMC-G) hybrid was prepared via a dual-template method shown in **Scheme 1**. Polystyrene microspheres (PS) (diameter ca. 150 nm) and a triblock polymeric surfactant (F127) were used as the hard template for macropores and the soft template for mesopores, respectively. Resol, the carbon precursor, and F127 were first dissolved in ethanol and impregnated into the aperture of PS hard templates; then, resol was cooperated with F127 surfactant micelles via an ethanol evaporation induced self-assembly (EISA) process to produce a 2D

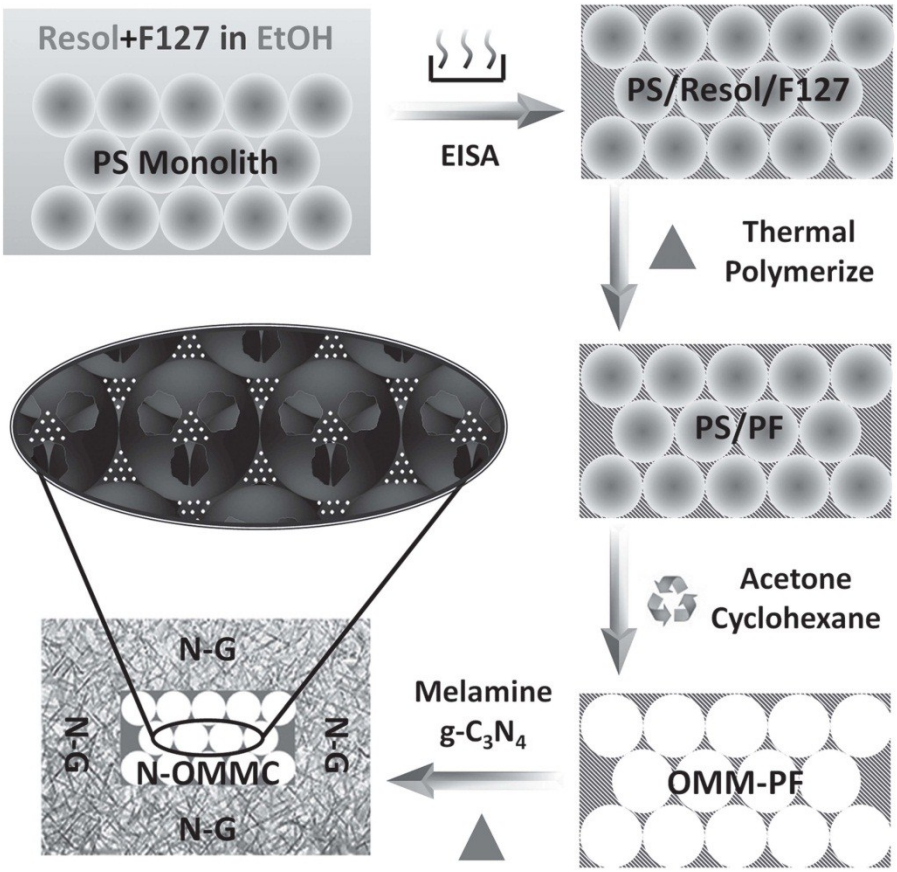

Scheme 1. Preparation processes of N-OMMC-G and the corresponding structure animation.

ordered mesostructure.[32] Following that, resol was thermally cross-linked into a rigid phenolic resin (PF), and the residual templates were subsequently washed off by a recyclable acetone and cyclohexane mixture, resulting in an ordered macro-mesoporous resin (OMM-PF). This resin was finely ground with melamine and graphitic carbon nitride (g-C_3N_4) in an agate mortar, and then heated up to 900 °C in N_2 to obtain the final N-OMMC-G. By contrast, nitrogen-doped macro-mesoporous carbon (N-OMMC) without the in-situ grown graphene could also be prepared by a similar heating process exept for separating the OMM-PF and melamine/g-C_3N_4 in individual quartz boats in the furnace tube. Nitrogen doped graphene (N-G) was also prepared by exfoliation of graphite and post doping processes for comparison.[7] (For details of the materials synthesis, please see Supporting Information)

The hybrid's microstructure was first characterized by scanning electron microscopy (SEM) and transmission electron microscopy (TEM). Overall, entangled foam-like graphene nanosheets are present in between the porous carbon micro blocks, interconnecting them to a network (**Figure 1**a, S1a-c). The pores of these carbon blocks consist of both 3D ordered macropores (ca. 150 nm, Figure 1b, S1d-f) and 2D mesopores located at the walls of the macropores (Figure 1c,d and S1g-i). The images of the graphene/carbon interface reveal the native in-situ growth of graphene from the porous carbon rather than the simple physical combination of two materials, indicating an excellent contact between them benefitting smooth electron transfer (Figure 1d and S1g-i). High resolution TEM observations reveal that these graphene nanosheets are composed of few single graphitic layers (Figure S1j-m). These nanosheets have also been investigated by atomic force microscopy (AFM) as shown in Figure 1f and S2. The corresponding AFM linear scans reveal that their thickness is ca. 1.5–2.5 nm, indicating 4–7 single graphitic layers in such in-situ formed graphene, in agreement with the TEM observations (Figure S1 j-m). Furthermore, the characteristic G band at ca. 1580 cm^{-1} in the microscopic Raman spectrum indicates the graphitic nature of this material (Figure S3).[23] Moreover, the small angle X-ray scattering pattern also confirms the existence of the 2D hexagonal mesochannels in this material (Figure S4).

The porosity of the materials was studied by means of nitrogen sorption technique (Figure 1g and S5). The nitrogen adsorption-desorption isotherms of N-OMMC-G disclose two distinct hysteresis loops at both medium (P/P_0 = 0.4–0.6) and high (P/P_0 = 0.85–1) pressure regions, which are attributed to the mesopores and neck sections of the spherical macropores. The rapid rise in the low pressure region also indicates the presence of micropores (Figure 1g inset). The mesopore

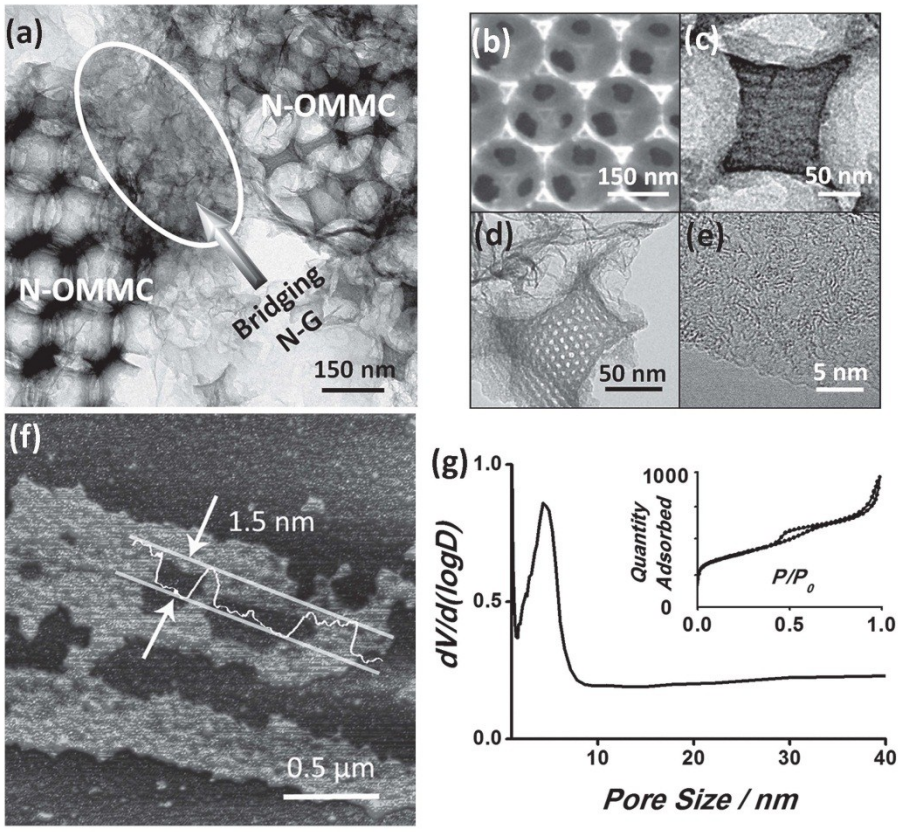

Figure 1. Typical structure characterizations of N-OMMC-G. (a-e) TEM and SEM images. (f) AFM image and corresponding linear scan of the in-situ formed graphene. (g) Pore size distribution and corresponding nitrogen sorption isotherms (inset).

diameter calculated by Barrett-Joyner-Halenda (BJH) method is ca. 4 nm, consistent with the TEM observations. Remarkably, the N-OMMC-G has an identical pore size distribution as its N-OMMC counterpart, with just a lightly lower specific surface area (1121 vs. 1360 $m^2 g^{-1}$), suggesting the in-situ formed graphene not to block the meso channels inside N-OMMC-G. The unique hierarchical pore structure composed of short-range mesopores located at the walls of large 3D ordered macropores is expected to maximize the number of accessible active sites as well as to facilitate the reactant transportation inside this material. On the contrary, N-G exhibits a wider pore size distribution (ca. 5–25 nm) and a much smaller specific surface area (ca. 160 $m^2 g^{-1}$), similar to other graphenes with "out-of-plane" pores provoked by the restacking of nanosheets.[7]

Nitrogen doping on N-OMMC-G was first detected by energy dispersive spectrometry (EDS) and further confirmed by Fourier transform infrared spectroscopy (Figure S6). The EDS elemental mappings of both graphene and porous carbon regions in N-OMMC-G (**Figure 2**a) show a homogeneous nitrogen distribution throughout the material. Regarding the complete decomposition of melamine and g-C_3N_4 at 900 °C,[7] it is reasonable to deduce that all the N signals originate from the N dopants. Detailed chemistry status of elements is further probed by X-ray photoelectron spectroscopy (XPS). The survey sweep shows similar element species of C, N and O in all samples and the N content in the samples is on a similar level (Figure 2b, S7b, e). High resolution XPS scans (inset of Figure 2b and Figure S7d, g) show that the N1s spectrum can be deconvoluted into three N species centered at ca. 401.2, 399.5 and 398.2 eV, corresponding to graphitic N, pyrrolic N and pyridinic N, respectively.[9,33] High resolution C1s spectra of the samples show typical carbon species in nitrogen doped carbons (Figure S7a,c,f).

Based on these observations, the formation mechanism of N-OMMC-G and the contribution of OMM-PF and melamine/g-C_3N_4 in the synthesis was revealed by comparing the preparation processes of different products (N-OMMC-G vs. N-OMMC) utilizing the same starting materials. It is reasonable to hypothesize that OMM-PF first acts as a precursor to form porous carbon in the thermal carbonization process. The carbonaceous gases released during the heating also serve as precursor for in-situ formed graphene. At the meantime, melamine undergoes thermal polymerization (<550 °C) to form layered g-C_3N_4 and releases nitrogenous gases. In this process, the carbonaceous gases released from OMM-PF are confined by as-formed g-C_3N_4, and the g-C_3N_4 serves as a template directing these carbonaceous gases to pyrolyze into graphene rather than other forms of carbon.[34] The released nitrogenous gases from g-C_3N_4 also serve as nitrogen dopant precursor for both graphene and porous carbon.[23,24] Increasing the temperature up

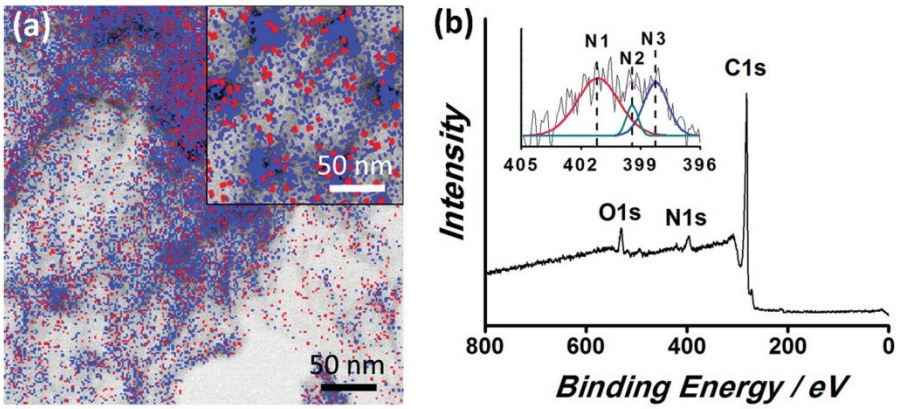

Figure 2. Elemental analysis of N-OMMC-G. (a) EDS elemental mapping showing distribution of N (red) and C (blue) atoms in graphene and porous carbon (inset) inside N-OMMC-G. (b) XPS sweap scan and high resolution N1s scan (inset).

to 900 °C leads to the decomposition of remaining g-C_3N_4 liberating the as-formed graphene present on the porous carbon. The decomposing g-C_3N_4 acts as a sacrificial nitrogen precursor to further dope the hybrid and also minimizes the nitrogen leaching from it at high temperature. From this aspect, the separation of melamine/g-C_3N_4 from OMM-PF into two boats during the heating process prohibited the capture of the carbonaceous gases inside the graphitic layers of g-C_3N_4 and thus, pristine N-OMMC could be obtained. In this procedure, the OMM-PF and melaimine/g-C_3N_4 served exclusively as porous carbon and nitrogen precursor respectively, which is also consistent with our proposed hypothesis.

Due to the inherent nitrogen species in this material, ORR was employed as an indicator reaction to evaluate the intrinsic advantages of this metal-free carbon based material for electrochemical processes. Cyclic voltammetry (CV) was first conducted on N-OMMC-G and comparative samples (N-OMMC, N-G; and their mixture, denoted as MIX) in both O_2 and N_2 saturated electrolytes (**Figure 3**a and S8). In the presence of N_2, only a featureless quasi-rectangular voltammogram was obtained;

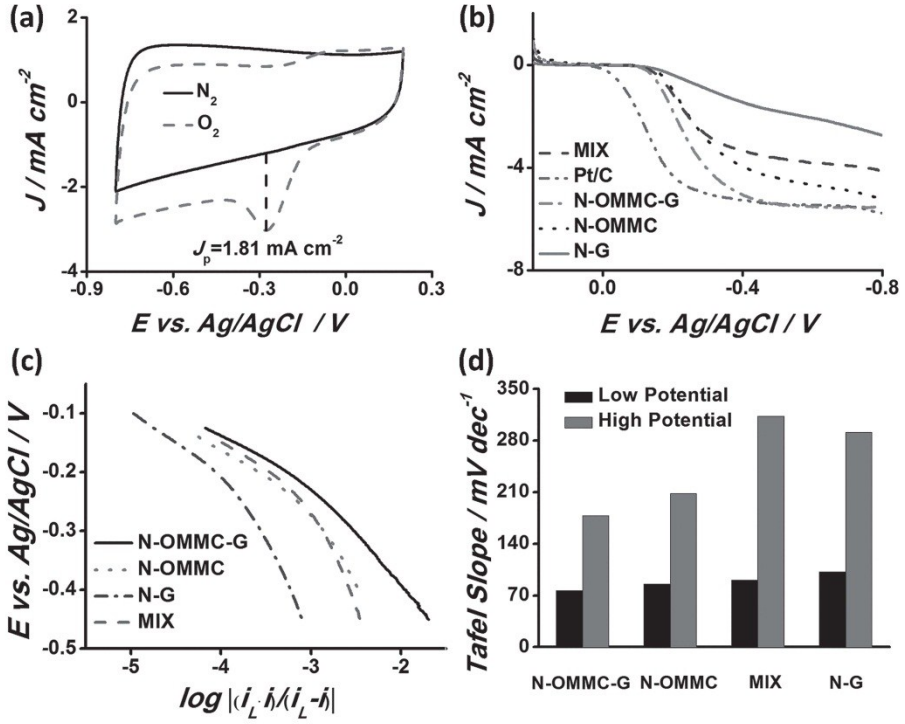

Figure 3. Oxygen electrochemical catalysis on N-OMMC-G. (a) CV in O_2 and N_2 saturated elelctrolyte. (b) LSVs of different samples at 1600 rpm. (c) Tafel plots of different samples and (d) the corresponding Tafel slope values.

whereas distinct ORR responses were observed on all samples in O_2 environment, suggesting their ability to electrochemically catalyze ORR. It is worth to note that N-OMMC-G shows the highest peak current of 1.81 mA cm^{-2}, which is significantly higher than that of the other samples, clearly suggesting its superior catalytic activity. Linear sweep voltammetries (LSVs) of all samples as well as the commercial Pt/C have been collected on a rotation disk electrode (RDE). Typically, increasing reaction currents were observed with increasing rotation speed due to the reduced diffusion distance (Figure S9a–e).[8,35] Despite the structure optimized N-OMMC-G shows a highly positive onset potential at ca. –0.05 V (Figure S9f), resembling that of previously reported graphene decorated with dual heteroelements or even metal particles,[7,16,29] it still does not outperform Pt/C (Figure 3b). Apart from the positive onset potential, N-OMMC-G possesses the highest diffusion-limited reaction current (J_D) similar as Pt/C (Figure 3b), suggesting a large number of exposed active sites on the material and a synergistic effect between N-doped graphene and porous carbon in this hybrid. The MIX sample, on the contrary, shows ORR current with values between the second highest N-OMMC and the lowest N-G (Figure 3b), which implies only a simple current overlap without any synergistic effects by mechanical mixing of N-OMMC and N-G. Besides, Koutecky-Levich (K-L) plots of N-OMMC-G are similar to that of Pt/C (Figure S10), which again confirms its excellent ORR activity. Furthermore, this metal-free N-OMMC-G shows a complete tolerance to methanol cross-over effect and excellent long term durability, which are superior to Pt/C and therefore render it a promising canditate for fuel cells or batteries (Figure S11).

To shed light on the origin of the synergistic effect and the intrinsic advantage of this advanced hybrid material, Tafel analysis was performed on these samples. The Tafel plots demonstrated two distinct linear regions at both low and high over potentials on all samples (Figure 3c and S12). The corresponding Tafel slope values are listed in Figure 3d. In the low over potential region, where the overall ORR process is controlled by the kinetics of the surface reactions,[36] N-OMMC-G gives the lowest value of 76.9 mV dec^{-1}, likely provoked by facilitated electron transfer by the native bridging graphene as well as its high surface area with the large number of active sites. In the high over potential region, on the other hand, where the reaction speed is dominated by the diffusion limitations inside the material, the Tafel slope of N-OMMC-G yields the lowest value again (178 mV dec^{-1}), closely followed by N-OMMC (208 mV dec^{-1}), revealing the apparently facilitated mass transfer inside this hierarchical porous material. Thus, considering the similar chemical component of the studied samples, the synergistically improved ORR catalytic activity of N-OMMC-G, compared with the analogues, can be reasonably attributed to the unique hierarchical pore architectures of the carbon micro blocks exposing the largest number of accessible active sites as well as the in-situ grown graphene present on the carbon blocks which serves as an electron channel enabling the rapid and sustainable reaction.

In conclusion, we have for the first time designed and constructed a novel hybrid material composed of natively grown graphene on hierarchical porous carbon through a very convenient bottom-up route, which successfully combines the advantages of both hierarchical porous carbon and graphene such as high surface area, large porous channel size, and high electron conductivity. Due to its excellent structural properties and inherent heteroatom dopants, this material itself can serve as an outstanding completely metal-free catalyst for ORR. The efficient electron transfer between carbon and the in-situ formed graphene makes its catalytic performance synergistically enhanced. Moreover, this carbon-based material could also potentially be used in other applications which require high surface area, high accessibly, and high conductivity.

Supporting Information

Supporting Information is available from the Wiley Online Library or from the author.

Acknowledgements

This research is financially supported by Australian Research Council (DP1095861, DP130104459).

Received: June 5, 2013
Revised: July 14, 2013
Published online: August 20, 2013

[1] R. Bashyam, P. Zelenay, *Nature* **2006**, *443*, 63.
[2] W. Z. Li, C. H. Liang, W. J. Zhou, J.S. Qiu Zhou, G. Q. Sun, Q. Xin, *J. Phys. Chem. B* **2003**, *107*, 6292.
[3] Y. G. Li, W. Zhou, H. L. Wang, L. M. Xie, Y. Y. Liang, F. Wei, J. C. Idrobo, S. J. Pennycook, H. J. Dai, *Nat. Nanotechnol.* **2012**, *7*, 394.
[4] Z. S. Wu, A. Winter, L. Chen, Y. Sun, A. Turchanin, X. L. Feng, K. Müllen, *Adv. Mater.* **2012**, *24*, 5130.
[5] A. Vinu, C. Streb, V. Murugesan, M. Hartmann, *J. Phys. Chem. B* **2003**, *107*, 8297.
[6] J. Wei, D. D. Zhou, Z. K. Sun, Y. H. Deng, Y. Y. Xia, D. Y. Zhao, *Adv. Func. Mater.* **2012**, *23*, 2322.
[7] J. Liang, Y. Jiao, M. Jaroniec, S. Z. Qiao, *Angew. Chem. Int. Ed.* **2012**, *51*, 11496.
[8] R. L. Liu, D. Q. Wu, X. L. Feng, K. Müllen, *Angew. Chem. Int. Ed.* **2010**, *49*, 2565.
[9] J. Liang, Y. Zheng, J. Chen, J. Liu, H. D. Jurcakova, M. Jaroniec, S. Z. Qiao, *Angew. Chem. Int. Ed.* **2012**, *51*, 3892.
[10] G. S. Chai, I. S. Shin, J. S. Yu, *Adv. Mater.* **2004**, *16*, 2057.
[11] S. L. Zhang, L. Chen, S. X. Zhou, D. Y. Zhao, L. M. Wu, *Chem. Mater.* **2010**, *22*, 3433.
[12] E. Antolini, *Appl. Catal. B: Environmental* **2009**, *88*, 1.
[13] H. Q. Li, Y. G. Wang, C. X. Wang, Y. Y. Xia, *J. Power Sources* **2008**, *185*, 1557.
[14] S. Y. Wang, L. P. Zhang, Z. H. Xia, A. Roy, D. W. Chang, J. B. Baek, L. M. Dai, *Angew. Chem. Int. Ed.* **2012**, *51*, 4209.
[15] S. Y. Wang, E. Iyyamperumal, A. Roy, Y. H. Xue, D. S. Yu, L. M. Dai, *Angew. Chem. Int. Ed.* **2011**, *50*, 11756.
[16] Y. Zheng, Y. Jiao, L. Ge, M. Jaroniec, S. Z. Qiao, *Angew. Chem. Int. Ed.* **2013**, *52*, 3110.
[17] P. Chen, T. Y. Xiao, Y. H. Qian, S. S. Li, S. H. Yu, *Advanced Materials* **2013**, *25*, 3192.
[18] P. Chen, J. J. Yang, S. S. Li, Z. Wang, T. Y. Xiao, Y. H. Qian, S. H. Yu, *Nano Energy* **2012**, *2*, 249.

[19] L. F. Chen, X. D. Zhang, H. W. Liang, M. G. Kong, Q. F. Guan, P. Chen, Z. Y. Wu, S. H. Yu, *ACS Nano* **2012**, *6*, 7092.
[20] Z. J. Fan, J. Yan, L. J. Zhi, Q. Zhang, T. Wei, J. Feng, M. Zhang, W. Z. Qian, F. Wei, *Adv. Mater.* **2010**, *22*, 3723.
[21] H. Sun, Z. Xu, C. Gao, *Adv. Mater.* **2013**, *25*, 2554.
[22] B. G. Choi, M. H. Yang, W. H. Hong, J. W. Choi, Y. S. Huh, *ACS Nano* **2012**, *6*, 4020.
[23] X. Li, S. Kurasch, U. Kaiser, M. Antonietti, *Angew. Chem. Int. Ed.* **2012**, *51*, 9689.
[24] X. H. Li, M. Antonietti, *Angew. Chem. Int. Ed.* **2013**, *52*, 4572.
[25] Z. S. Wu, Y. Sun, Y. Z. Tan, S. B. Yang, X. L. Feng, K. Mullen, *J. Am. Chem. Soc.* **2012**, *134*, 19532.
[26] S. L. Chou, J. Z. Wang, M. Choucair, H. K. Liu, J. A. Stride, S. X. Dou, *Electrochem. Commun.* **2010**, *12*, 303.
[27] J. K. Lee, K. B. Smith, C. M. Hayner, H. H. Kung, *Chem. Commun.* **2010**, *46*, 2025.
[28] H. Hu, Z. B. Zhao, W. B. Wan, Y. Gogotsi, J. S. Qiu, *Adv. Mater.* **2013**, *25*, 2219.
[29] Z. S. Wu, S. B. Yang, Y. Sun, K. Parvez, X. L. Feng, K. Mullen, *J. Am. Chem. Soc.* **2012**, *134*, 9082.
[30] Y. W. Zhu, S. Murali, M. D. Stoller, K. J. Ganesh, W. W. Cai, P. J. Ferreira, A. Pirkle, R. M. Wallace, K. A. Cychosz, M. Thommes, D. Su, E. A. Stach, R. S. Ruoff, *Science* **2011**, *332*, 1537.
[31] Z. J. Fan, Q. K. Zhao, T. Y. Li, J. Yan, Y. M. Ren, J. Feng, T. Wei, *Carbon* **2012**, *50*, 1699.
[32] Y. Meng, D. Gu, F. Q. Zhang, Y. F. Shi, H. F. Yang, Z. Li, C. Z. Yu, B. Tu, D. Y. Zhao, *Angew. Chem. Int. Ed.* **2005**, *44*, 7053.
[33] Y. Zheng, Y. Jiao, J. Chen, J. Liu, J. Liang, A. Du, W. M. Zhang, Z. H. Zhu, S. C. Smith, M. Jaroniec, G. Q. Lu, S. Z. Qiao, *J. Am. Chem. Soc.* **2011**, *133*, 20116.
[34] Z. W. Liu, F. Peng, H. J. Wang, H. Yu, W. X. Zheng, J. Yang, *Angew. Chem. Int. Ed.* **2011**, *50*, 3257.
[35] W. Yang, T. P. Fellinger, M. Antonietti, *J. Am. Chem. Soc.* **2011**, *133*, 206.
[36] M.T. de Groot, M. Merkx, A. H. Wonders, M. T. M. Koper, *J. Am. Chem. Soc.* **2005**, *127*, 7579.

3.3 Supplimentary Ingormation

This section is included in the thesis as as a supplimentary information to setion 3.2. It includes additional information which is not put in the main text of the published papr, but as an electronic sullimentrary information freely accessable online.

N-doped Graphene Natively Rooted on Hierarchical Ordered Porous Carbon for Enhanced Oxygen Reduction

By *Ji Liang, Xin Du, Gibson Christopher, Xi Wen Du, Shi Zhang Qiao**

[*] Prof. Shi Zhang Qiao, Ji Liang, Dr. Xin Du
School of Chemical Engineering, the University of Adelaide,
Adelaide, SA 5005, Australia
E-mail: s.qiao@adelaide.edu.au
Dr. Gibson Christopher
Centre for Nanoscale Science and Technology,
School of Chemical and Physical Sciences, Flinders University,
Adelaide, SA 5043, Australia
Prof. Xi Wen Du
School of Materials Science and Engineering, Tianjin University,
Tianjin, 300072, China

I. Experimental Section

1. Chemicals

Graphite flakes, sulfuric acid (H_2SO_4, 95-98 %), potassium permanganate ($KMnO_4$, 99 %), phosphorus pentoxide (P_2O_5, 98 %), potassium persulfate ($K_2S_2O_8$, 99 %), colloidal silica (Ludox HS-40, 40 wt. % water suspension), melamine (99 %), hydrofluoric acid (HF, 48 %), styrene (ST, 99 %), polyvinyl pyrrolidone (PVP, MW 44000, 99 %), sodium hydroxide (NaOH, 99 %), ethanol (EtOH, absolute), phenol (99 %), formaldehyde solution (37 wt. %), hydrochloric acid (38 wt. %) were purchased from Sigma-Aldrich and directly used without further treatment or purification.

2. Preparation of polystyrene (PS) spheres

13 ml ST was firstly washed with 4 ml 10 wt. % NaOH aq for three times and then deionized (DI) water for two times to remove the stabilizer. During this process, the ST changed from color-less into light yellow, indicating the complete removal of the stabilizer. Then, ST was added to 100 ml DI water containing 0.5 g PVP in a triple-neck flask. The mixture was flux-stirred at 70 °C/600 rpm

for 30 min with continuous N_2 purged in. Then, 20 ml aqueous solution containing 0.3 g $K_2S_2O_8$ was injected into the flask to initiate the polymerization of ST into PS. The mixture was kept flux-stirred at 70 °C/600 rpm for another 24 h. The milky product was then centrifuged and washed with EtOH for three times. Finally, the PS microspheres dispersed in EtOH was dried in an evaporation dish, resulting in a colorful 3D packed PS template.

3. Preparation of resol

Typically, 10 g of phenol was heated until melt at 42 °C in a sealed bottle. Then 2.1 g of 20 % NaOH aqueous solution was added by drop with continuous stir at 100 rpm. Afterward, 17.7 g of 37 wt. % formaldehyde solution was added by drop and the heating temperature was raised to 70 °C. The solution was heated and stirred for another 1 h, and then cooled to room temperature. After that, the pH of the solution was adjusted with 2 M HCl aqueous solution until 7. Then, water was removed by rotary evaporation and the product was diluted into a 20 wt. % EtOH solution. During the dilution, the separated NaCl was then filtered, resulting in a pale yellow solution.

4. Preparations of N-OMMC-G and N-OMMC

0.3 g F127 was dissolved in 5 ml EtOH at 35 °C with continuous stir for 30 min. Then 1.5 g of above prepared 20 wt. % resol solution was added and kept stirred for another 20 min. The above solution was added by drop into an evaporation dish with 1.4 g of packed PS template. After all the solution was added, the dish was kept under vacuum until no bubble came out from the PS template. Then, the mixture was tried in air overnight forming PS/Resl/F127. After that, the material was heated at 100 °C for 24 h in air and then at 350 °C in N_2 for 4 h with a ramp rate of 1 °C min^{-1}. The obtained brown solid (PS/PF) was washed in excessive amount of acetone and cyclohexane mixture (1:1 *vol*) at 60 °C twice under continuous stir to remove the residual template. The washing solvent could be recycled by rotary evaporation. The solid (OMM-PF) was filtered and dried at 100 °C overnight; and color from revered opal structure could be observed. OMM-PF was finely ground with 10 times weight of melamine and g-C_3N_4 (prepared by heating melamine in air at 550 °C for 4 h) (1:1 *wt.*) in an agate mortar and the mixture was heated in the following program in N_2 to prepare N-OMMC-G:

Room temperature → 60 °C (ramp rate: 1 °C min^{-1}, kept for 2 h) → 600 °C (ramp rate: 1 °C min^{-1}, kept for 4 h) → 900 °C (ramp rate: 5 °C min^{-1}, kept for 3 h) → room temperature

To prepare N-OMMC without *in-situ* formed graphene, 5 times weight of melamine was wrapped with aluminum foil and put in another boat beside the boat containing OMM-PF. The two boats were heated following the program below in N_2:

Room temperature → 60 °C (ramp rate: 1 °C min^{-1}, kept for 2 h) → 600 °C (ramp rate: 1 °C min^{-1}, kept for 4 h) → room temperature

Then, the obtained carbon and 5 times of g-C_3N_4 in another boat were heated again at 900 °C for 3 h in N_2 with a ramp rate of 5 °C min^{-1} to obtain the final N-OMMC.

5. Preparation of chemically converted N-G

Graphene oxide (GO) was prepared through the modified Hammer's method. GO was dispersed into DI water to obtain a 0.05 wt.% suspension. 5 g of colloidal silica (as the hard template to form the "out-of-plain" mesopores) containing 40 wt. % 12 nm silica nanospheres was added to 200 ml of the GO suspension. Then, the mixture was rotary evaporated resulting in a crisp brown film. Afterwards, the solid was slightly crashed in a motar with 0.5 g melamin into fine power, and then heated at 900 °C for 1 h under the protection of Ar to obtain N-G/SiO_2. The as-prepared sample was finally washed with HF acid to remove the silica, followed by water washing and drying at 100 °C.

6. Characterizations

Nitrogen adsorption-desorption isotherm was recorded on Tristar II (Micrometrics) at -196 °C. Pore size distribution was obtained by Barrett-Joyner-Halenda (BJH) model using adsorption branch data of the nitrogen isotherms. The specific surface area was calculated using adsorption data at the relative pressure range of P/P_0 = 0.05-0.3 by Brunauer-Emmett-Teller model.

Microstructures of the samples were observed on TEM (Tecnai G2 Spirit TEM) and SEM (Quanta FEG 450, FEI). High resolution TEM images were obtained on JEM-2100 microscopy. Elemental mapping was conducted using EDAX detector attached on JEM-2100. Small Angle X-ray scattering measurement was conducted on Rigaku D/max 2500 V/PC (Rigaku, Japan). Fourier transform infrared spectroscopy was obtained on Nicolet 6700 FT-IR (Thermal Scientific, US).

XPS analysis was carried out on AXIS Ultra spectrometer (Kratos Analytical Ltd., GB) with monochromated Al Kα radiation at a pressure of *ca.* 5×10^{-9} Pa. Binding energies were calibrated using the adventitious carbon (C1s) = 284.5 eV

All Raman spectra were collected in air using a Witec confocal Raman Microscope (Alpha 300RS, Germany) equipped with a 532 nm laser diode (<60 mW). A CCD detector (cooled to -60 °C) was used to collect Stokes Raman signals under a ×40 objective (Nikon) at room temperature (*ca.* 24 ◦C) in a wavenumber range of 0 to 2000 cm^{-1} with an integration time of 0.5 or 5 s for each measurement.

AFM images were acquired in ambient conditions with a Multimode and NanoScope V controller (Digital Instruments, Bruker, US) using NSC15 silicon probes (Mikromasch, US) operating in tapping mode. These probes have a fundamental resonance frequency between 250 and 400 kHz, nominal spring constant of 42 N m^{-1} and nominal tip radius of 10 nm. Amplitude set-points were typically 70 to 90% of the cantilever free amplitude. Topographic height images were obtained at a scan rate of 1 Hz simultaneously with feedback controls optimized for each sample. All images represent flattened data using the NanoScope Analysis version 1.20 software packages.

The conductivity of the samples were tested on a homemade mold with two round electrodes connected to a digital multi meter (Agilent 34401A, US). The samples were tested under the same constant pressure with the same contact area with the electrode. The thickness of the tested sample

was recorded with a caliper. Each sample was tested for 3 times and the average resistivity (R) was listed below, which were obtained by dividing the measured resistance with thickness.

	N-OMMC-G	N-OMMC	MIX	N-G
R (Ω/mm)	2.7	5.79	3.43	4

Interestingly, the N-G showed a relatively high apparent resistance, which might be due to its highly loose structure, which is harder to be compressed and to form close contact between the nanosheets.

7. Electrochemical test

For the electrochemical test, 2 mg of each sample was dispersed in 1 ml of deionized water (18.2 MΩ). The mixture was ultrasonicated to obtain a homogenous catalyst ink.

To prepare the working electrode for electrochemical measurements, 40 µl of the ink was dipped on a mirror polished glass carbon electrode (0.192 cm^2) and dried at room temperature in air. Then, the working electrode was inserted into the cell setup, which is composed of a platinum counter electrode, an Ag/AgCl/KCl (3 M) reference electrode and a 125 ml glass cell containing 100 ml of electrolyte.

Cyclic voltammetry (CV) experiments were performed on an electrochemical analysis station (CHI 760 C, CH Instruments, USA) at 50 mV s^{-1}. Before test, an O_2/N_2 flow was used through the electrolyte in the cell for 20 min to saturate it with O_2/N_2. The cell was kept in a 25 ºC water bath for all the electrochemical tests.

For the rotating disk electrode (RDE) test, the same working electrode was prepared as for CV and the test was conducted on CHI 760 C. A Pt wire and an Ag/AgCl/KCl (3 M) were used as the counter and reference electrodes, respectively. The linear sweep voltammograms of the modified glass carbon electrode were recorded in O_2 saturated 0.1 M KOH with a scan rate of 5 mV s^{-1} at various rotating speeds from 400 to 2000 rpm for ORR. After each scan, the electrolyte was saturated with O_2 again for 20 minutes. The sample was tested 2 times to avoid any incidental error.

The Koutecky-Levich plots were obtained by linear fitting of the reciprocal rotating speed versus reciprocal current density collected at different potentials form -0.4 V to -0.8 V. The overall electron transfer numbers per oxygen molecule involved in a typical ORR process weere calculated from the slopes of Koutecky-Levich plots using the following equation:

$$1/j_D = 1/j_k + 1/B\omega^{1/2}$$

where j_k is the kinetic current in amperes at a constant potential, ω is the electrode rotating speed in rpm, and B, the reciprocal of the slope, which was determined from the slope of Koutecky-Levich plots based on Levich equation as followed:

$$B = 0.2\, nFA\nu^{-1/6}C_{O2}D_{O2}^{2/3}$$

where n is the number of electrons transferred per oxygen molecule, F is the Faraday constant （96485 C mol^{-1}）, D_{O2} is the diffusion coefficient of O_2 in 0.1 M KOH (1.9×10^{-5} cm s^{-1}), *v* is the kinetic viscosity (0.01013 cm^2 s^{-1}), and C_{O2} is the concentration of O_2 (1.2×10^{-3} mol L^{-1}). The constant 0.2 is adopted when the rotating speed is in rpm.

According to this equation, the electron transfer numbers of the metal free samples were listed in the table below:

	-0.4 V	-0.5 V	-0.6 V	-0.7 V	-0.8 V
N-OMMC-G	3.16	3.29	3.34	3.41	3.53
N-OMMC	2.67	2.81	2.93	3.11	3.41
MIX	2.67	2.84	3.01	3.23	3.51
N-G	1.95	2.16	2.31	2.48	2.75

II. Supplementary Results

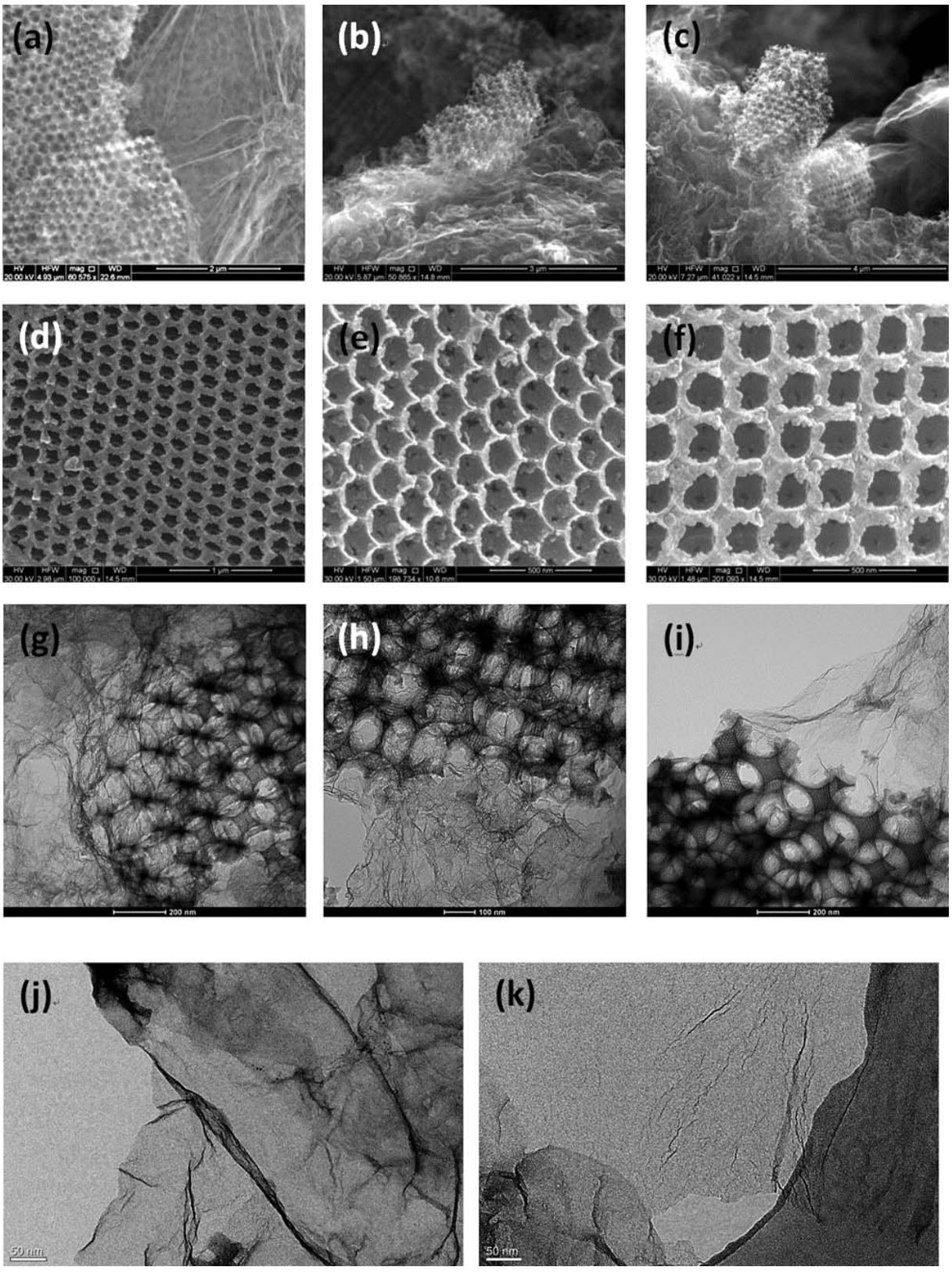

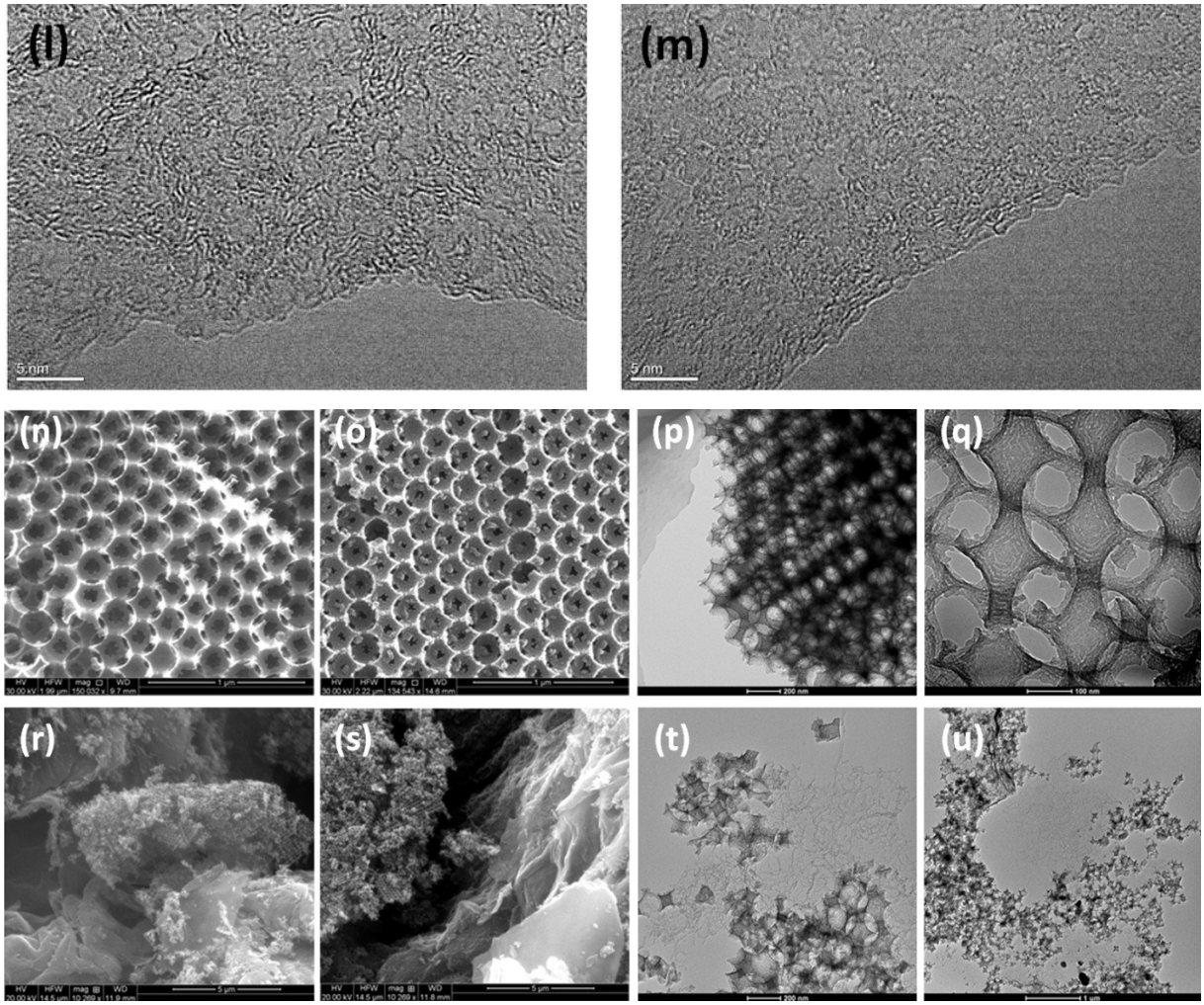

Figure S1. SEM and TEM images of N-OMMC-G. (a-c) SEM observations showing the homogeneous distribution of in-situ formed graphene connecting the porous carbon micro blocks inside the N-OMMC-G hybrid. (d-f) High magnification SEM images showing the ordered macropores on N-OMMC-G micro blocks. (g-i) TEM images of the joint sections between graphene and porous carbon in N-OMMC-G, showing the native growth of graphene from carbon. (j-k) TEM images of the graphene sections in N-OMMC-G at both low and high resolutions. (l-m) High resolution TEM images of the graphene section in N-OMMC-G. (n-o) SEM images of N-OMMC and (p-q) TEM images of N-OMMC. (r-s) SEM images of MIX and (t-u) TEM images of MIX.

It is worth to note that the images clearly show a different structure between the *in-situ* formed hybrid (N-OMMC-G) and the physically mixed material (N-OMMC/G, denoted as MIX). Due to the large aspect ratio of the chemically exfoliated graphene, it is very easy to aggregate during the drying (either to normally dry at room atmosphere or to freeze dry at very low temperature). Thus it needs long time to grind the N-OMMC and N-G to form a relatively homogeneous mixture (MIX), thus the structure of the N-OMMC in MIX could be partially broken during this process as shown in Figure S1n-q, which on the contrary shows the advantages of our one-step *in-situ* growth of

graphene on porous carbon materials.

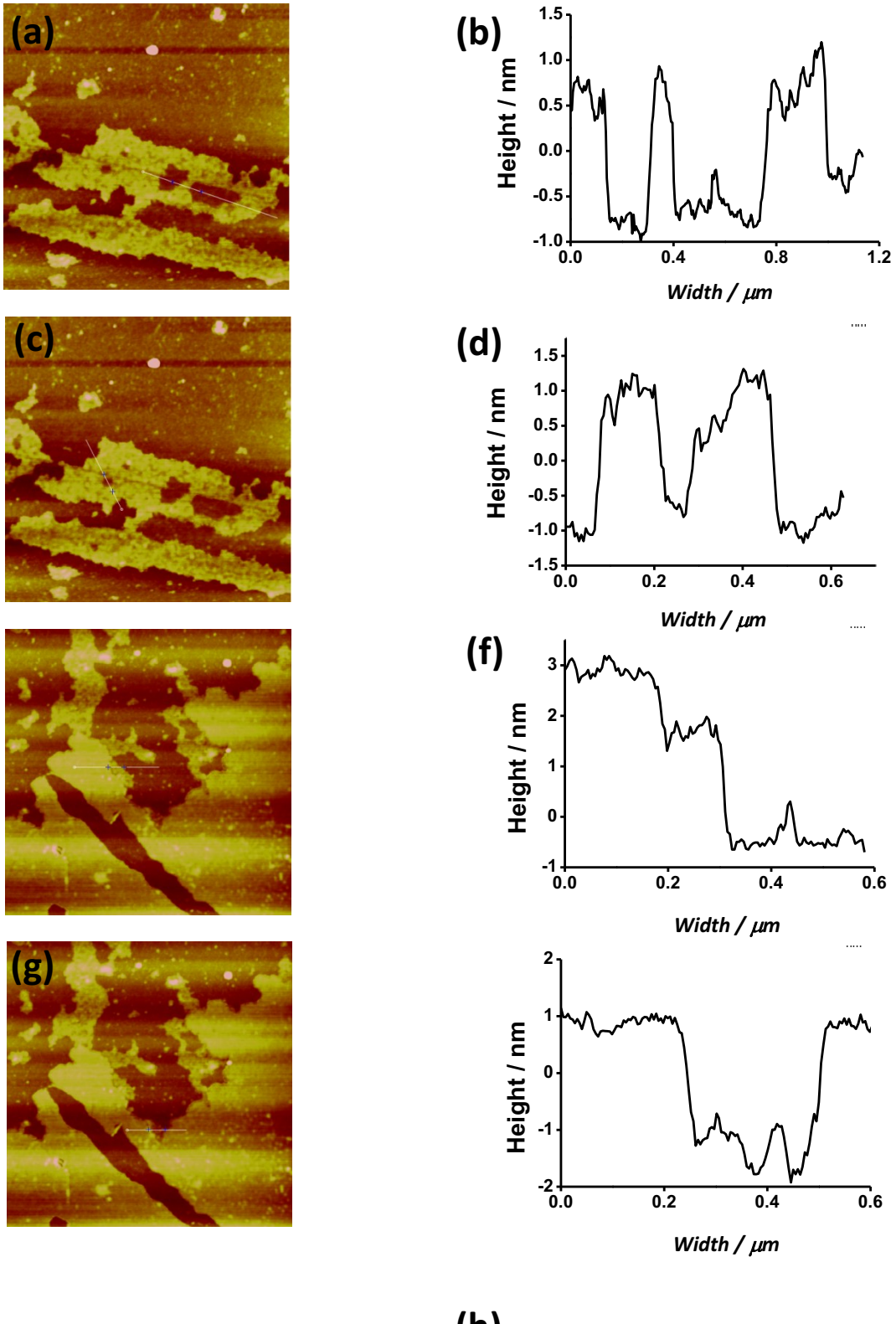

Figure S2. AFM images of the graphene in N-OMMC-G (a, c, e, g) and the corresponding linear scans (scan regions shown in the AFM images) showing the thickness of these nanosheets (b, d, f, g).

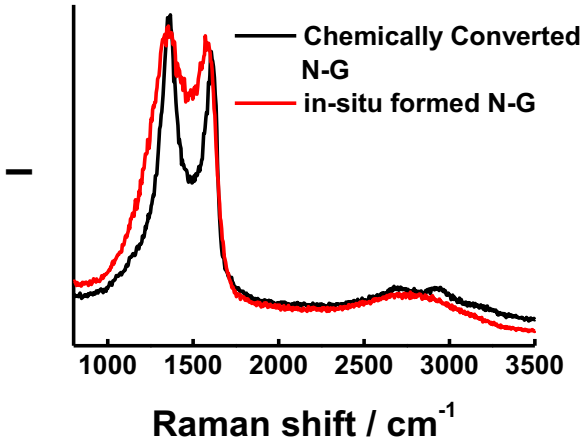

Figure S3. Microscopic Raman spectra of *in-situ* formed graphene (red) and chemically converted N-G (black).

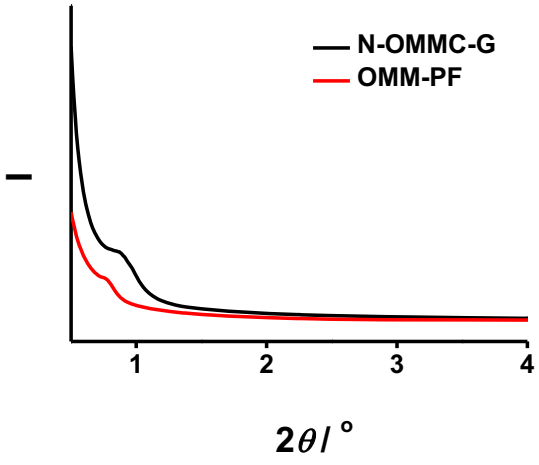

Figure S4. SAXS curves of N-OMMC-G and OMM-PF.

The SAXS of N-OMMC-G and OMM-PF are quite similar, indicating the mesostructure has been maintained after the high temperature heating process. Only one peak has been observed on both materials, which is possible due to the short range nature of the mesopores (less than 100 nm) in this material.

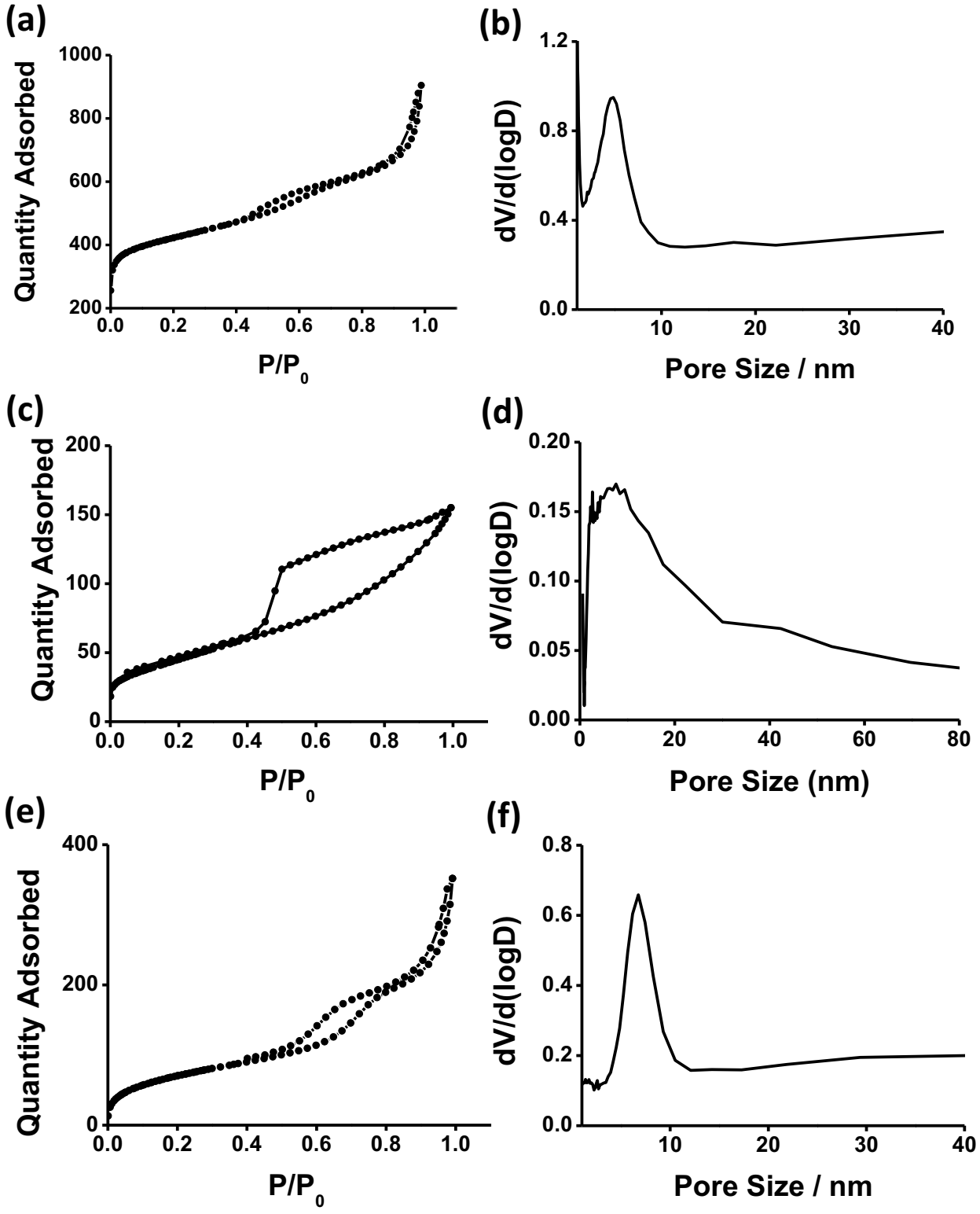

Figure S5. Nitrogen adsorption-desorption isotherms and the corresponding pore size distribution of N-OMMC (a, b); chemically converted N-G (c, d); and OMM-PF (e, f).

The surface area of OMM-PF is *ca.* 258 m^2/g and its pore size distribution (centered at *ca.* 6.7 nm) is slightly larger than the final carbon materials (N-OMMC and N-OMMC-G), which results from a pore shrinkage after the carbonization of the polymers, but the hierarchical porous structure has been successfully remained as shown from the similar isotherms.

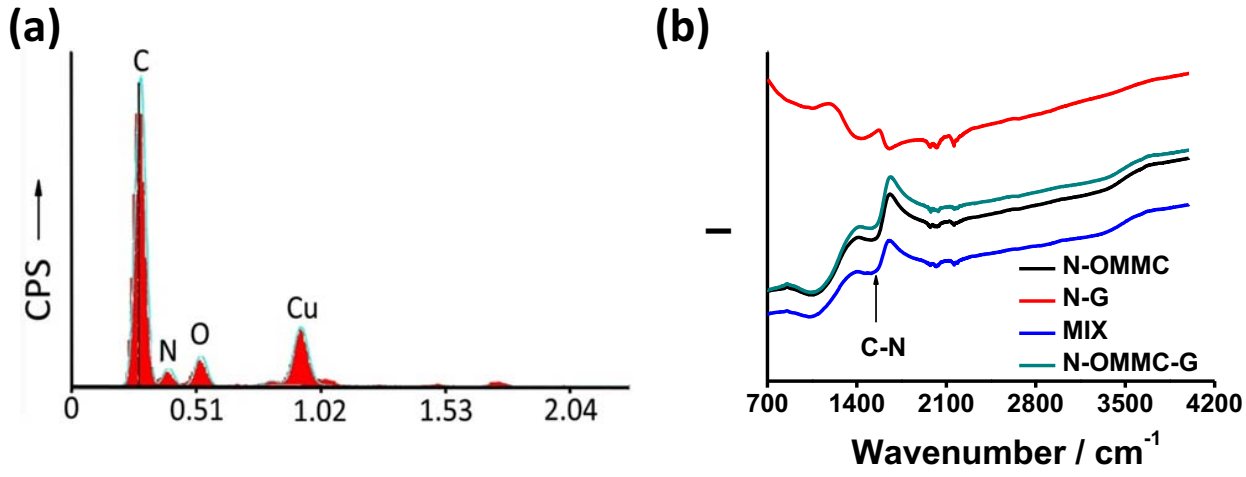

Figure S6. (a) EDS analysis of N-OMMC-G and (b) FTIR analysis of the samples.

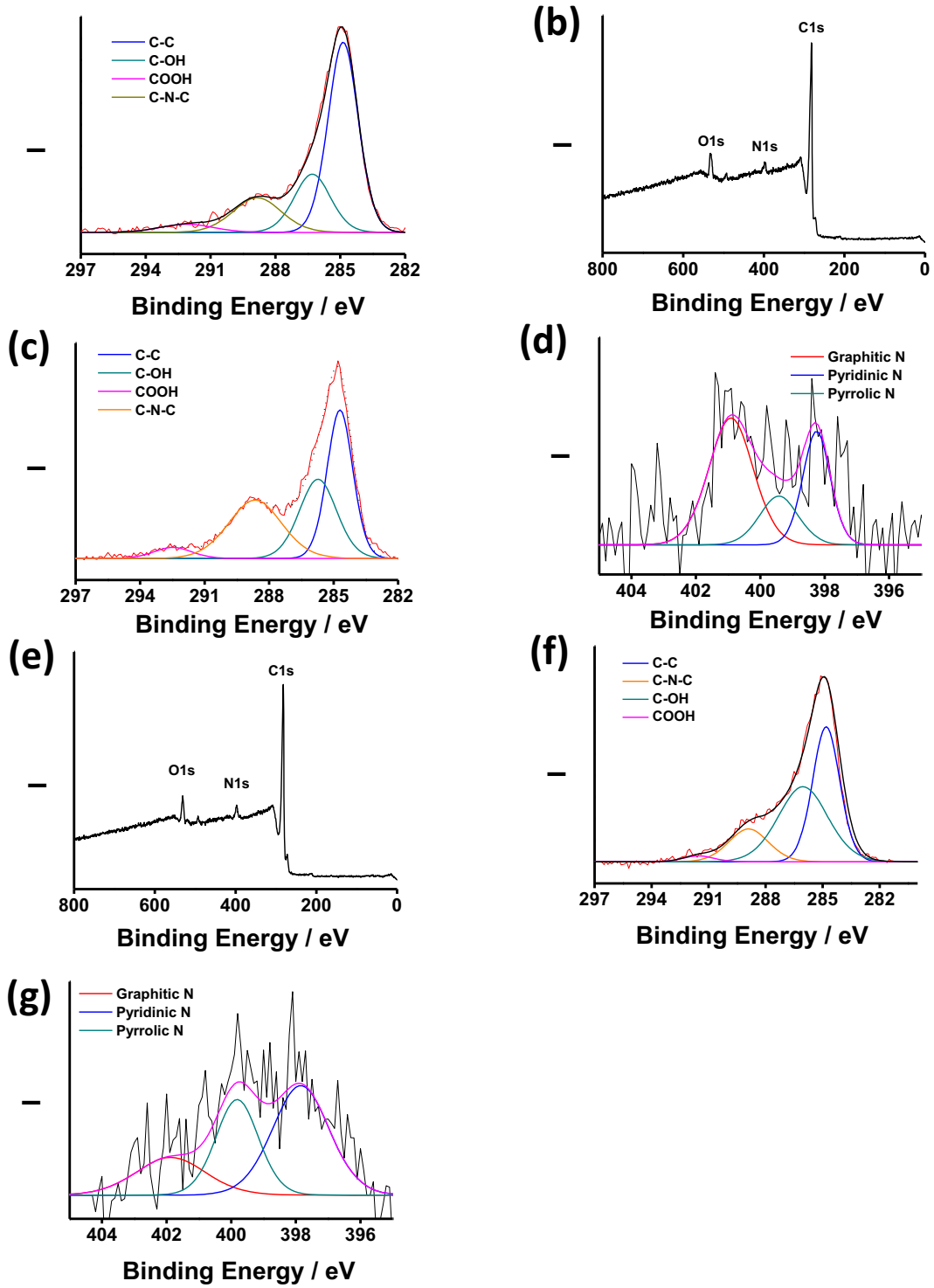

Figure S7. Additional XPS results of the materials. (a) High resolution C1s spectrum of N-OMMC-G. (b, c, d) Survey scan spectrum, high resolution C1s and N1s spectra of N-OMMC, respectively. (e, f, g) Survey scan spectrum, high resolution C1s and N1s spectra of N-G, respectively.

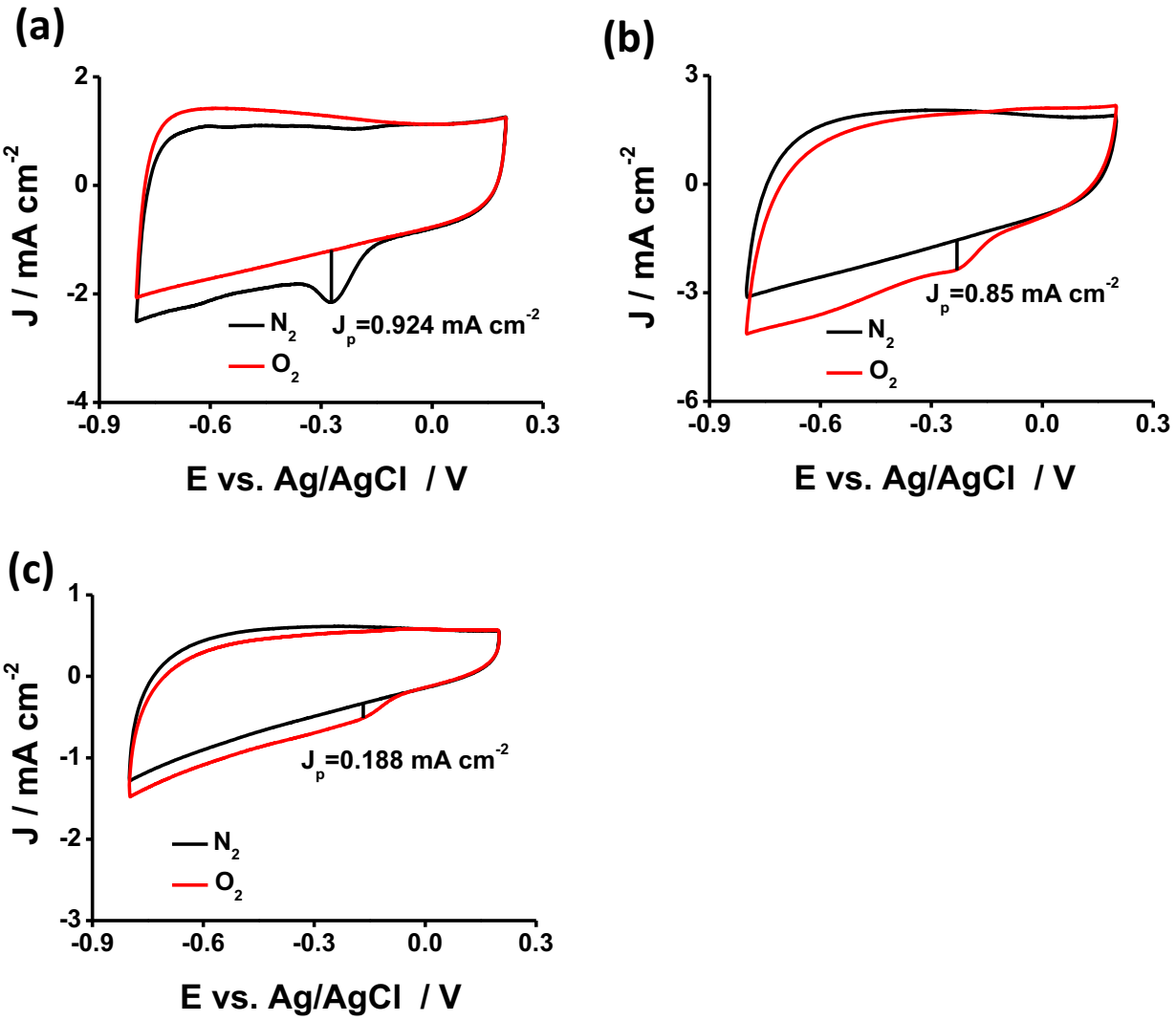

Figure S8. CV tests of N-OMMC (a), MIX (b) and N-G (c), conducted in N_2 and O_2 saturated 0.1 KOH aqueous solution.

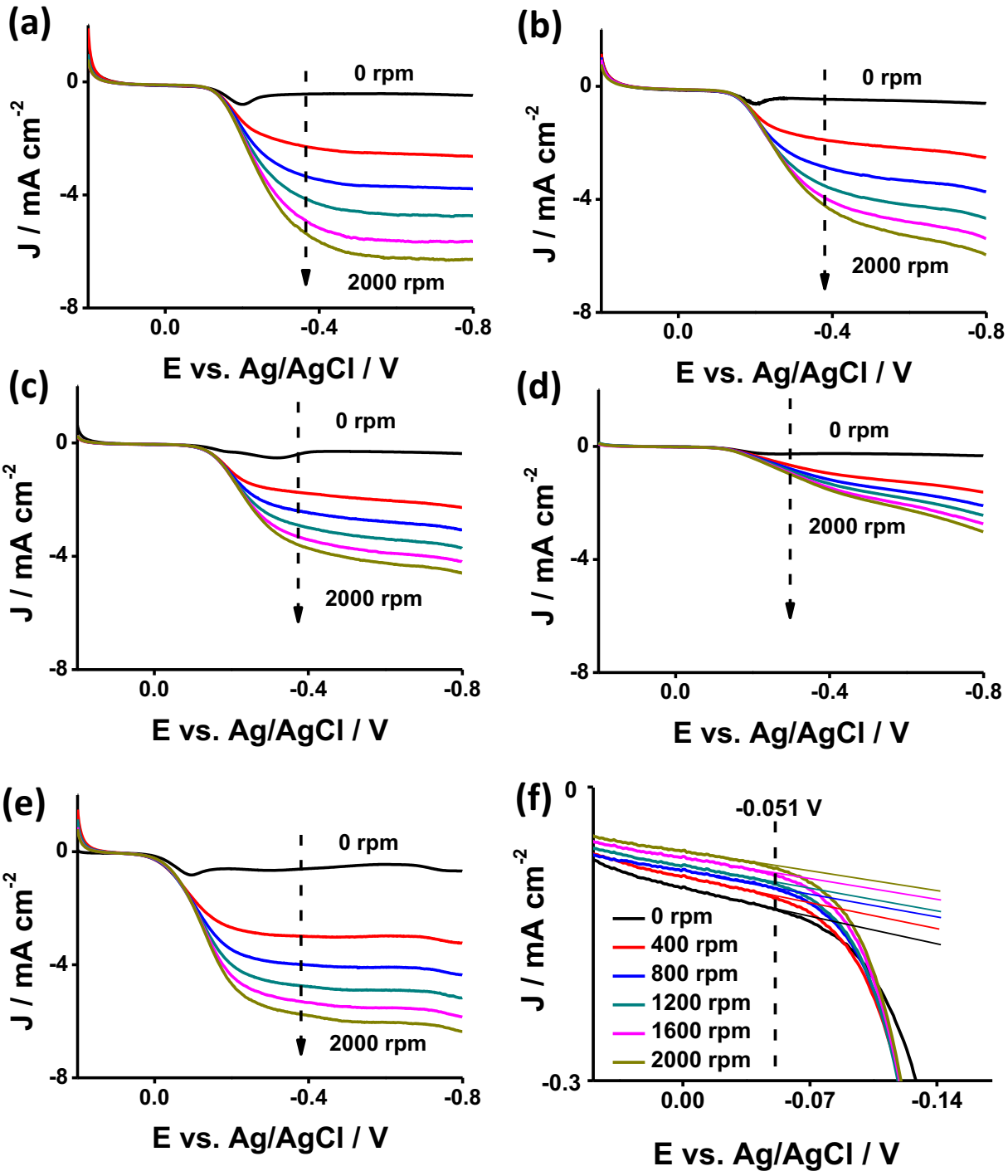

Figure S9. LSVs of N-OMMC-G (a), N-OMMC (b), MIX (c), N-G (d) and Pt/C (e) at 0-2000 rpm with an increment of 400 rpm between neighboring LSV curves. (f) Enlarged section of the LSVs of N-OMMC-G at different rotation speeds showing the ORR onset potential at *ca.* -0.051 V vs. Ag/AgCl.

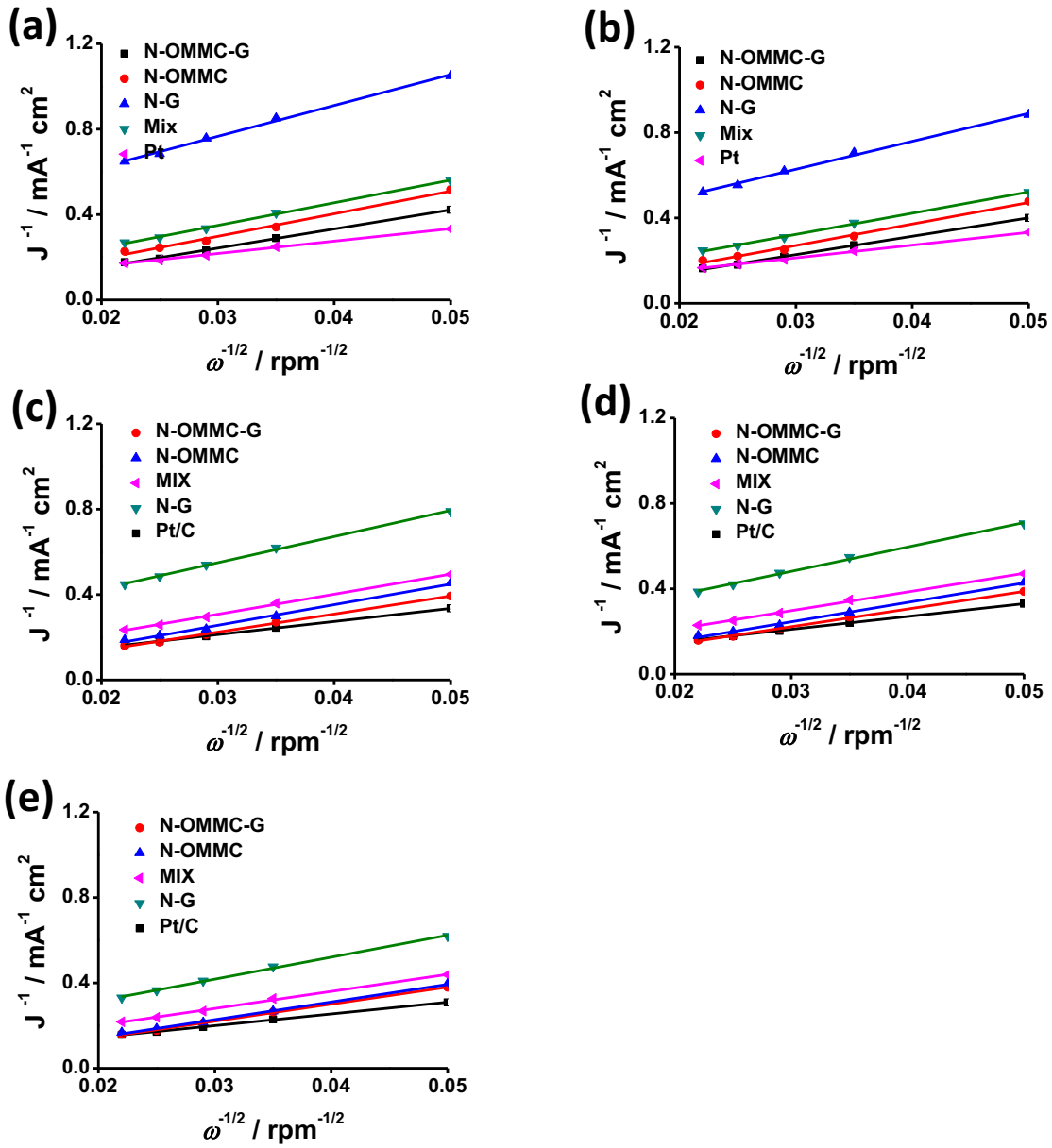

Figure S10. K-L plots of different samples at different potentials vs. Ag/AgCl. (a) -0.4 V. (b) -0.5 V. (c) -0.6 V. (d) -0.7 V. (e) -0.8 V. The electron transfer numbers (n), calculated from the slopes of the K-L plots of each carbon sample, are around *ca.* 2-3.5, similar as the values previously obtained on N doped carbon materials. Among these values, the N-OMMC-G gives the largest n, which means relatively larger amount of O_2 is reduced via the more efficient 4 electron pathway.

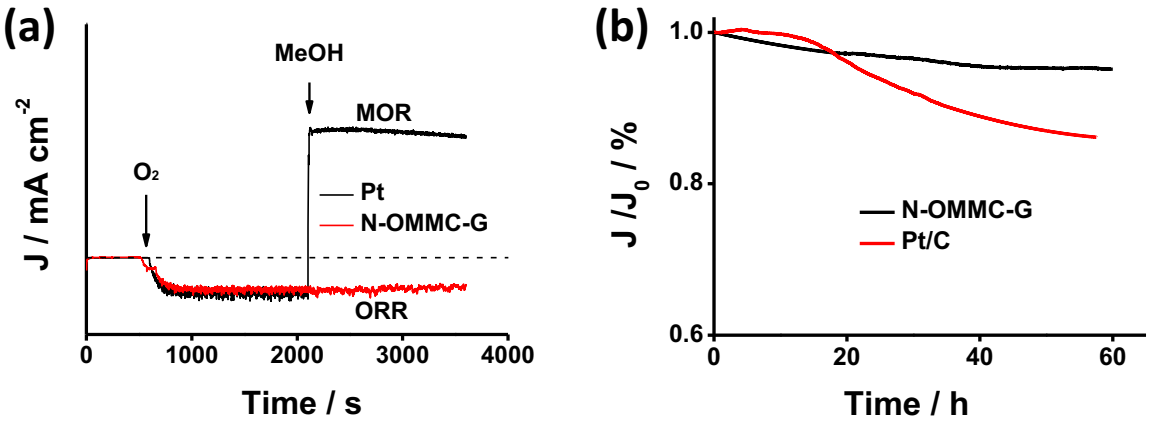

Figure S11. (a) Methanol cross-over toleration test of N-OMMC-G and Pt/C in 0.1 M KOH aqueous solution. (b) 60 h durability test of N-OMMC-G and Pt/C in O_2 saturated 0.1 M KOH aqueous solution.

The higher stability of N-OMMC-G compared with the Pt/C could be possiblily attributed to several aspects including: 1) good thermal stability coming from the high heating temperature during the preparation for a relatively long period of time; 2) 3-D ordered carbon skeleton which not only faciliate the mass diffusion, but also provide a good mechanical stability.

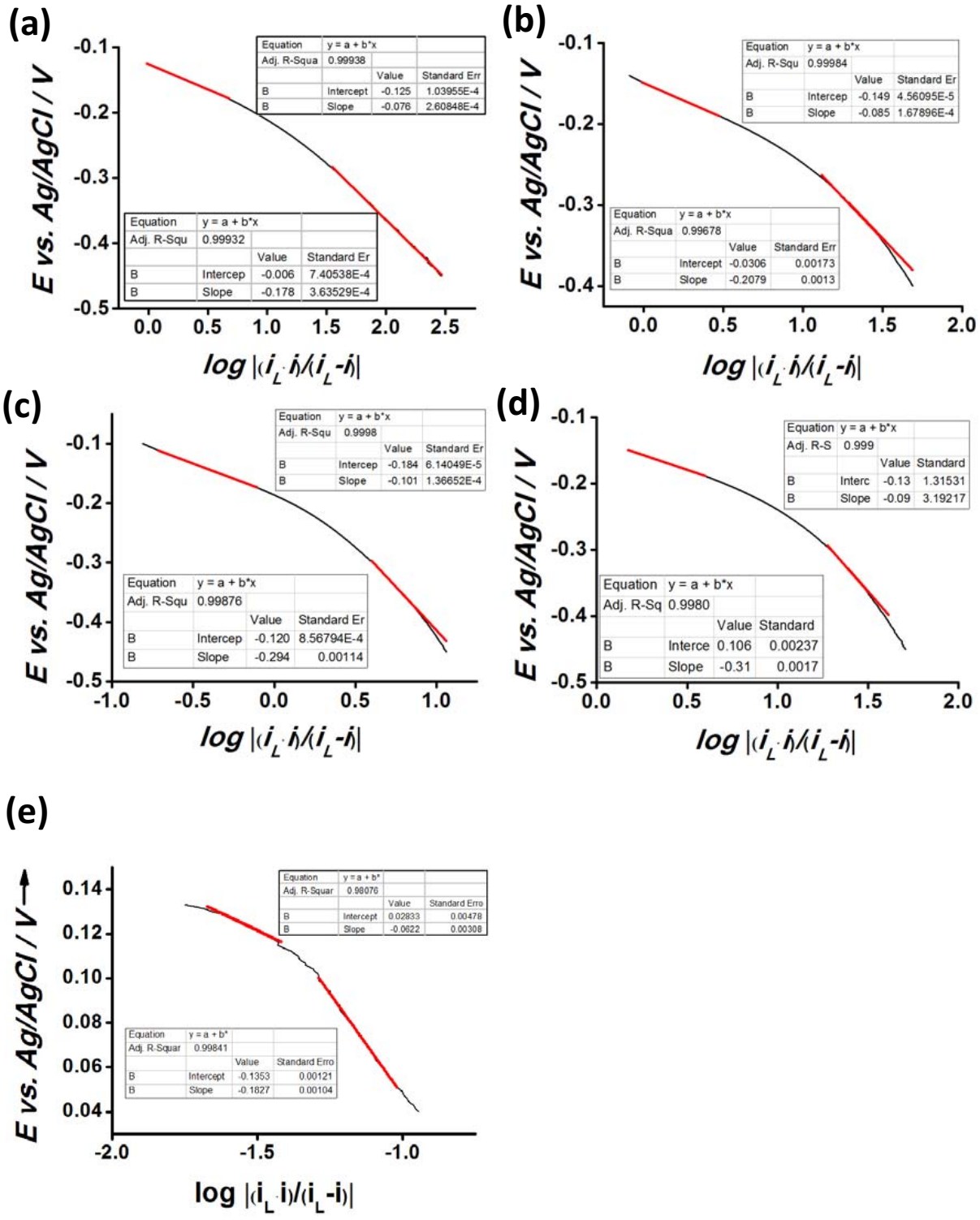

Figure S12. Tafel plots of the samples obtained from the LSVs at 1600 rpm. (a) N-OMMC-G. (b) N-OMMC. (c) MIX. (d) N-G. (e) Pt/C.

The Tafel plots demonstrates two distinct linear regions at both low and high over potentials on all samples. In the low over potential regions where the overall ORR process is controlled by the speed of surface reactions, the N-OMMC-G gives the lowest value of 76.9 mV dec^{-1} compared with N-OMMC (85.7 mV dec^{-1}), N-G (101.8 mV dec^{-1}) or the MIX (90.9 mV dec^{-1}). The lower value of N-OMMC-G compared with N-OMMC could be reasonably attributed to the more facile electron

transfer by the native bridging graphene, while the highest value on N-G would come from the smallest number of exposed active sites due to its lowest surface area. Besides, the intermediate value of MIX again clearly reveals simply mechanical mixing cannot bring synergistic performance enhancement to the material. On the other hand at high over potential region where the reaction speed is dominated by the diffusion limitations inside the material, the Tafel slope of N-OMMC-G is 178 mV dec^{-1}, which is closely followed by N-OMMC (208 mV dec^{-1}) and significantly lower than the values of MIX (313 mV dec^{-1}) and N-G (291.4 mV dec^{-1}). The low Tafel slope value of N-OMMC-G and N-OMMC at high over potential further confirms the apparently more facile mass transfer inside this hierarchical porous material. Interestingly, the MIX has the highest Tafel slope value, suggesting its highest mass transfer resistance, which indicates pore blockage of N-OMMC by N-G after mechanical mixing.

The Tafel slope value of Pt/C has also been obtained based on the similar conditions as mentioned above. The values show *ca.* -60 mV dec^{-1} and *ca.* -180 mV dec^{-1} at low and high over potential, respectively, which are typical of multi crystal Pt nanoparticles loaded on porous carbons for ORR in KOH electrolytes. [1]

Ref:

[1] C. F. Zinola, A. M. Castro Luna, W. E. Triaca, A. J. Arvia, Journal of Applied Electrochemistry 1994, 24, 531.